



ACADEMIC
PRESS

Available online at www.sciencedirect.com

SCIENCE @ DIRECT®

Journal of Computational Physics 184 (2003) 266–298

JOURNAL OF
COMPUTATIONAL
PHYSICS

www.elsevier.com/locate/jcp

Second-order sign-preserving conservative interpolation (remapping) on general grids

L.G. Margolin^a, Mikhail Shashkov^{b,*}

^a *Center for Nonlinear Studies, Los Alamos National Laboratory, Mail Stop B258, Los Alamos, NM 87545, USA*

^b *Theoretical Division, T-7, Los Alamos National Laboratory Mail Stop B284, Los Alamos, NM 87545, USA*

Received 15 April 2002; accepted 10 October 2002

Abstract

An accurate conservative interpolation (remapping) algorithm is an essential component of most arbitrary Lagrangian–Eulerian (ALE) methods. In this paper we describe a local remapping algorithm for a positive scalar function. This algorithm is second-order accurate, conservative, and sign preserving. The algorithm is based on estimating the mass exchanged between cells at their common interface, and so is equally applicable to structured and unstructured grids. We construct the algorithm in a series of steps, clearly delineating the assumptions and errors made at each step. We validate our theory with a suite of numerical examples, analyzing the results from the viewpoint of accuracy and order of convergence.

© 2002 Elsevier Science B.V. All rights reserved.

Keywords: Conservative interpolation; Remapping; ALE methods

1. Introduction

In numerical simulations of fluid flow, the choice of the computational grid is crucial. Traditionally, there have been two viewpoints, utilizing the Lagrangian or the Eulerian framework, each with its own advantages and disadvantages. In a pioneering paper, Hirt et al. [14] developed the formalism for a grid whose motion could be determined as an independent degree of freedom and showed that this general framework could be used to combine the best properties of Lagrangian and Eulerian methods. This class of methods has been termed arbitrary Lagrangian–Eulerian or ALE. Many authors have described ALE strategies to optimize accuracy, robustness, or computational efficiency, see for example [2,4,15,17, 19,23,29].

It is possible to use the ALE formalism to run in a mainly Lagrangian mode, with an occasional rezone/remap whenever the grid becomes too distorted. However, it is generally more effective to rezone and remap on each cycle, a strategy termed continuous rezoning.

* Corresponding author. Tel.: +1-505-667-4400; fax: +1-505-665-5757.

E-mail address: shashkov@lanl.gov (M. Shashkov).

It is possible to formulate the ALE scheme as a single algorithm [7] based on solving the equations in a moving coordinate frame. However it is more usual to separate it into three separate phases. These are: (1) a Lagrangian phase in which the solution and grid are updated; (2) a rezoning phase in which the nodes of the computational grid are moved to a more optimal position; and (3) a remapping phase in which the Lagrangian solution is interpolated onto the rezoned grid. One advantage of continuous rezone is that the individual grid movements can be constrained to be small, allowing the use of a local remapper where mass (and other conserved quantities) is only exchanged between neighboring cells. Local remappers are logically simpler and computationally more efficient than global remappers, where an explicit or implicit overlay of the two arbitrary meshes is required [8–10,13].

The main goal of this paper is to describe a new remapping algorithm for use in continuous rezone ALE simulations. Typically, local ALE remappers are constructed by adapting advection algorithms, for which there is a huge literature, cf. [1,2,4–6,11,22,25,26,28,29]. However, the connection between the advection equation and conservative remapping does not appear to be well understood; in particular, the underlying assumptions and discretization errors of using advection methods for remapping are not easily identified. In this paper, we will construct our remapping algorithm without reference to advection.

We will proceed in a series of steps, with the assumptions and errors of each step clearly delineated. The final result will be a second-order accurate algorithm, fully conservative, and sign preserving (e.g., if the original quantity is everywhere positive, then the remapped quantity will be everywhere positive). Our algorithm is face based, implying that it is equally applicable to structured and unstructured grids. To validate our theory, we will perform a suite of two-dimensional (2D) examples (the results of extensive testing of our method in (1D) examples and additional (2D) examples can be found in [24]), and will analyze the results both for accuracy and order of convergence.

Although we make no reliance on advection theory, we do borrow one idea from the advection literature. The MPDATA schemes [31,32] employ an upwind estimate to compensate the second-order error. By construction, such compensation is sign-preserving and leads to fully second-order accurate schemes. We have found that this technique to be equally effective in compensating remapping error.

A precise estimate of the remap error is essential for error compensation. However it has an additional use that is not so obvious and deserves brief mention. The goal of the rezoner is to move the mesh to reduce the overall error of the simulation. This can be achieved within the rezoning algorithm by formulating an error functional, which is a function both of the Lagrangian solution and of the grid geometry, and then minimizing this functional by moving the grid. In this context, the reduction of the Lagrangian error must be weighed against the additional error resulting from the remapping.

An outline of this paper is as follows. We begin in Section 2 by carefully defining the issues and goals of a remapping scheme. In Section 3, we will build a framework for remapping, based on a partition of the volume of a new (i.e., rezoned) cell in terms of its overlap with the old (i.e., Lagrangian) cells. We will show that different remap schemes result from the details of the reconstruction of the discrete density function. We will then reformulate these schemes in terms of generalized face fluxes, thus simplifying the task of ensuring exact conservation. In Section 4, we will show that the volume integral over a new cell can be expressed as the volume integral over the old cell plus a sum of surface integrals (line integrals in 2D) over the regions covered (swept) by the displacement of the cell faces – i.e., the “swept regions”. Based on this decomposition, we will define a first-order accurate “exact” donor cell, and an “approximate” donor-cell remapping algorithm. Both methods use a piecewise constant reconstruction of the density; in the approximate method, we will further simplify the computation of the integrals over the swept regions by considering only the two densities adjacent to the face. This last approximation eliminates the need for detailed calculations of the intersections of the sides of the new and the old grids. In Section 5, we will analyze the error of the approximate donor cell algorithm, and devise a method to

compensate error depending on the sign of the swept regions. The resulting algorithm is positivity preserving, and has overall second-order accuracy.

In Section 6 we will present two-dimensional simulations in which several known functions are re-mapped on different sequences of grids, including unstructured grids. We will show the results graphically and analyze them from the viewpoints of accuracy and order of convergence. We will summarize our results in Section 7.

2. Background and rationale

2.1. Grids

We consider a two-dimensional computational domain Ω , assumed to be a general polygon. We assume that we are given a mesh on Ω that consists of cells C_i , $i = 1, \dots, i_{\max}$ that cover Ω without gaps or overlaps. The cells C_i can be nonconvex.

Each cell is defined by a set of vertices (which we will sometimes call points), denoted by $P(C_i)$, and a set of sides (which are segments of straight lines), denoted by $F(C_i)$. Each side F_k is shared by only two cells, denoted by $C(F_k)$. Each vertex P_m may be shared by an arbitrary number of cells. We denote the set of cells that have a common vertex by $C(P_m)$; similarly, we denote the set of all sides sharing a common vertex P_m by $F(P_m)$. The cells that share a side or vertex with a particular cell are called *neighbors*; the set of all the neighbors of a cell C_i , is denoted $C(C_i)$. The reciprocal relation of neighborhood defines the *connectivity* of the grid.

Let P_a, P_b, P_c, \dots be points. We denote the line segment joining two points by $\{P_a, P_b\}$. When three or more points are listed within the curly brackets, we denote the closed figure defined by the points in the order prescribed. For example, $\{P_a, P_b, P_c\}$ is a triangle.

In the context of ALE methods, we consider two grids with the same connectivity – i.e., the same number of cells and vertices, and the same neighbor relations. The grid that contains the cells C_i is called the Lagrangian or *old* grid. The second grid, containing the cells \tilde{C}_k , is called the rezoned or *new* grid. In the ALE method, the rezoned grid results from an algorithm (i.e., a rezoner) that identifies and mitigates inadequacies of the Lagrangian grid. In Figs. 1 and 2, we show examples of a Lagrangian grid (solid lines) and a rezoned grid (dashed lines). The rezoned grids were generated using the optimization-based reference Jacobian strategy described in [16]. The rezoned grid produced by this algorithm remains “close” to Lagrangian grid, but has better geometrical quality. Fig. 2 illustrates how complicated the relative locations of the two grids can be even when displacements of the nodes are small.

After rezoning, the old mesh $\{C_i\}$ is mapped into a new mesh $\{\tilde{C}_i\}$. We define a set $\mathcal{C}(C_i) = \cup_k C_k$, such that

$$\tilde{C}_i \in \mathcal{C}(C_i). \quad (2.1)$$

For any two grids, such a set exists because $\tilde{C}_i \in \cup_{k=1}^{i_{\max}} C_k$. However we will always consider the minimal set for which (2.1) holds. We note that the new remapping method that we will describe in this paper does not require any explicit knowledge of $\mathcal{C}(C_i)$. For the rezoning method described in [16] $\mathcal{C}(C_i) = C_i \cup C(C_i)$; that is, the new cell \tilde{C}_i is contained in the union of the old cell C_i , and its immediate neighbors, see, for example, Fig. 2(b).

In this paper, we will require a minimal regularity of the grid. In particular, we will assume there exists a small parameter h that characterizes the average cell size, and that tends to zero as the grid is refined. We further assume that there exist constants, independent of h , such that the length of any side, l_i , and the (2D) volume of any cell, V_i satisfy

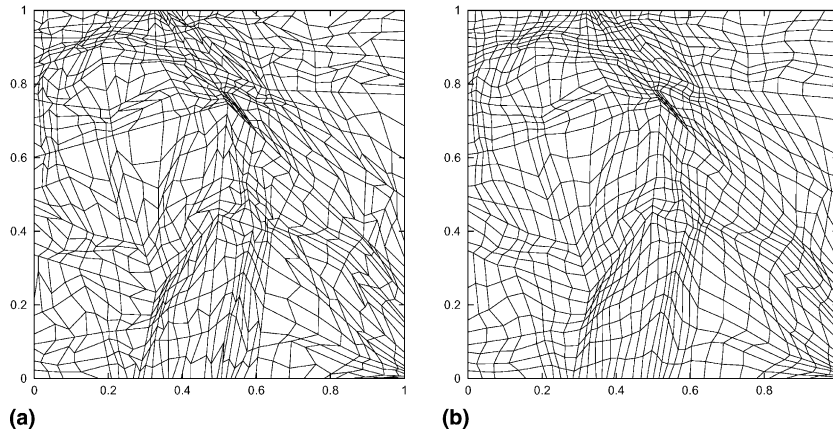


Fig. 1. (a) Old (Lagrangian) grid; (b) new (rezoned) grid.

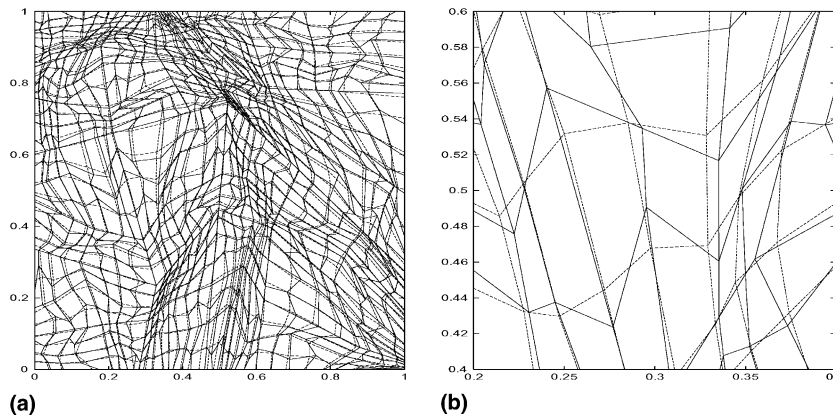


Fig. 2. Lagrangian and rezoned grid: (a) entire region; (b) fragment.

$$c_L h \leq l_i \leq C_L h, \quad c_V h^2 \leq V(C_i) \leq C_V h^2.$$

2.2. Notation

In this paper, we will describe several different remapping schemes. To distinguish among them consistently, we adopt the following notation. We will write all physical quantities (e.g., the density ρ or the mass m) on the old (Lagrangian) grid with no superscript, whereas the presence of any superscript indicates the quantity on the new (remapped) grid. We will use the superscript ex for the “exact” value, the superscript de for the exact donor-cell scheme described in Section 3, the superscript da for the “approximate” donor cell scheme described in Section 4, and the superscripts mc, mm, and mb for the multipass schemes described in Section 5. On occasion, we will write formulas that apply for any choice of superscript, and then we use the generic symbol *.

2.3. Statement of the remapping problem

We assume that there is a positive function $\rho(\vec{\mathbf{r}}) > 0$, $\mathbf{r} = (x, y, z)$, which we call density. that is defined throughout the problem domain. The only information that we are given about this function is its mean value in each of the cells of the old grid:

$$\rho_i = \frac{\int_{C_i} \rho(\mathbf{r}) dV}{V(C_i)}, \quad (2.2)$$

where $V(C_i)$ is the volume of the cell C_i . The numerator of (2.2) is the cell mass:

$$m_i \equiv \int_{C_i} \rho(\mathbf{r}) dV, \quad (2.3)$$

and so the density is:

$$\rho_i = \frac{m_i}{V(C_i)}. \quad (2.4)$$

The total problem mass is

$$M \equiv \int_{\Omega} \rho(\mathbf{r}) dV = \sum_{i=1}^{i_{\max}} \int_{C_i} \rho(\mathbf{r}) dV = \sum_{i=1}^{i_{\max}} m_i = \sum_{i=1}^{i_{\max}} \rho_i V(C_i). \quad (2.5)$$

The problem statement is to find accurate approximations m_i^* for the masses of the new cells

$$m_i^* \approx m_i^{\text{ex}} = \int_{\tilde{C}_i} \rho(\mathbf{r}) dV. \quad (2.6)$$

The issue is to define what is meant by “accurate”, since the underlying density field is not known in detail. We will consider mathematical smoothness and physical realizability of the density to quantify accuracy. There are constraints that the new cell masses must obey that follow from the positivity of the density function and from global conservation of the total mass. In particular, we require that all m_i^* are positive, $m_i^* > 0$. We also require

$$\sum_{i=1}^{i_{\max}} m_i^* = M, \quad (2.7)$$

a statement of global conservation. Because each cell mass is positive, global conservation implies that m_i^* is bounded from above. This can be taken as a definition of stability for remapping.

The approximate mean values of density in the new cells are defined by

$$\rho_i^* = \frac{m_i^*}{V(\tilde{C}_i)}. \quad (2.8)$$

The positivity of m_i^* implies $\rho_i^* > 0$ in the new cells. We will refer to the problem of finding accurate, bounded approximations for the masses and the corresponding mean densities on the new mesh, such that total mass is conserved, as *positivity-preserving remapping*, or alternately, as *positivity-preserving conservative interpolation*.

We append a remark about the underlying density function, whose existence we have postulated. Although such a function may be assumed to be uniquely specified at the beginning of a problem, this uniqueness will vanish as the numerical simulation progresses. More generally at any problem time, we will

define a class of continuous functions whose volume integrals over the cells are the cell masses, and which are smooth in the sense that their third derivatives in space, properly nondimensionalized, are bounded. When we refer to an exact solution, we mean any member of this class.

3. Cell-intersection-based donor-cell method

Each cell of the new mesh \tilde{C}_i is formed from pieces of the cells of the old mesh C_i

$$\tilde{C}_i = \bigcup_{k=1}^{i_{\max}} (\tilde{C}_i \cap C_k) = \bigcup_{k \in \mathcal{C}(C_i)} (\tilde{C}_i \cap C_k). \tag{3.1}$$

A natural approach to remapping can be based on the preceding representation of the new cell:

$$\int_{\tilde{C}_i} \rho(\mathbf{r}) dV = \sum_{k \in \mathcal{C}(C_i)} \int_{\tilde{C}_i \cap C_k} \rho(\mathbf{r}) dV. \tag{3.2}$$

This formula would be exact if we knew the density function everywhere on the old mesh. However, as pointed out earlier, we only know the average value of $\rho(\mathbf{r})$ within a cell. Thus it is necessary to reconstruct the density function.

The simplest reconstruction is to assume that density is piecewise constant, and equal to the given cell average for each cell of the old mesh. Then

$$\int_{\tilde{C}_i \cap C_k} \rho(\mathbf{r}) dV \approx \rho_k \cdot V(\tilde{C}_i \cap C_k). \tag{3.3}$$

This leads to the following formula for the remapped masses on the new mesh:

$$m_i^{\text{de}} = \sum_{k \in \mathcal{C}(C_i)} \rho_k \cdot V(\tilde{C}_i \cap C_k). \tag{3.4}$$

We will refer to the remapping method of (3.4) as cell-intersection-based donor-cell (CIB/DC) method. The CIB acronym reminds us that we have as yet made no approximations to the areas of overlap between the cells of the old and new meshes. The DC acronym arises from the idea that the old cell donates a portion of its mass to the new cell, estimated from piecewise constant reconstruction of the density. The DC terminology is used for similar approximations of the advection equation.

The CIB/DC method preserves the positivity of the mass field, because m_i^{de} is defined by the summation of nonnegative pieces. The new mean density is

$$\rho_i^{\text{de}} = \sum_{k \in \mathcal{C}(C_i)} \rho_k \cdot \frac{V(\tilde{C}_i \cap C_k)}{V(\tilde{C}_i)}. \tag{3.5}$$

Clearly each coefficient of ρ_k in this formula is positive. Furthermore

$$\sum_{k \in \mathcal{C}(C_i)} V(\tilde{C}_i \cap C_k) = V(\tilde{C}_i) \tag{3.6}$$

so that the sum of the coefficients of ρ_k is unity. It follows that

$$\min_{k=1}^{i_{\max}} \rho_k \leq \min_{k \in \mathcal{C}(C_i)} \rho_k \leq \rho_i^{\text{de}} \leq \max_{k \in \mathcal{C}(C_i)} \rho_k \leq \max_{k=1}^{i_{\max}} \rho_k; \tag{3.7}$$

i.e., the approximate new mean densities are bounded, and no new local extrema are created. The CIB/DC method is conservative because

$$\begin{aligned} \sum_{i=1}^{i_{\max}} m_i^{\text{de}} &= \sum_{i=1}^{i_{\max}} \left(\sum_{k \in \mathcal{C}(C_i)} \rho_k \cdot V(\tilde{C}_i \cap C_k) \right) = \sum_{i=1}^{i_{\max}} \left(\sum_{k=1}^{i_{\max}} \rho_k \cdot V(\tilde{C}_i \cap C_k) \right) \\ &= \sum_{k=1}^{i_{\max}} \left(\sum_{i=1}^{i_{\max}} \rho_k \cdot V(\tilde{C}_i \cap C_k) \right) = \sum_{k=1}^{i_{\max}} \left(\rho_k \cdot \sum_{i=1}^{i_{\max}} V(\tilde{C}_i \cap C_k) \right) = \sum_{k=1}^{i_{\max}} (\rho_k \cdot V(C_k)) \\ &= \sum_{k=1}^{i_{\max}} m_k = M. \end{aligned} \tag{3.8}$$

The CIB/DC method is just one of the methods that can be based on (3.2). The conservativeness of such methods is guaranteed whenever the reconstruction of density within the old cell preserves its mean value, and the overlap volumes between the old and new cells are calculated exactly. However, to assure the positivity of density for an arbitrary new mesh, the reconstructed density must be positive everywhere within each cell of the old mesh. This is not an easy task and generally requires special procedures that limit the variability of the density. We refer the interested reader to [3,18] and the references therein, where the process of reconstruction is considered in the framework of solving advection equations. We note that CIB methods are very general and in principle can be applied when the old and new grids are not related to each other – even may have different number of cells of arbitrary shapes and different connectivity. CIB/DC is only first-order accurate for a smooth function $\rho(\mathbf{r})$. It does preserve a constant density field. Appropriate piecewise linear reconstruction may lead to a second-order accurate method. Note that CIB methods require finding all intersections between the cells of the old and new grids.

When the old and new grids have the same connectivity, we can reformulate the CIB/DC method based on the following representation of new cell:

$$\tilde{C}_i = C_i \cup \left(\bigcup_{k \in \mathcal{C}'(C_i)} \tilde{C}_i \cap C_k \right) \setminus \left(\bigcup_{k \in \mathcal{C}'(C_i)} C_i \cap \tilde{C}_k \right), \tag{3.9}$$

where

$$\mathcal{C}'(C_i) = \mathcal{C}(C_i) \setminus C_i, \tag{3.10}$$

and where \setminus is difference operation on sets. In words, the new cell is the old cell plus pieces of neighboring cells that are added minus pieces of the old cell lost to other new cells. The corresponding representation for the exact mass of the new cell is

$$\begin{aligned} m_i^{\text{ex}} &= \int_{\tilde{C}_i} \rho(\mathbf{r}) dV = \int_{C_i} \rho(\mathbf{r}) dV + \sum_{k \in \mathcal{C}'(C_i)} \int_{\tilde{C}_i \cap C_k} \rho(\mathbf{r}) dV - \sum_{k \in \mathcal{C}'(C_i)} \int_{C_i \cap \tilde{C}_k} \rho(\mathbf{r}) dV \\ &= m_i + \sum_{k \in \mathcal{C}'(C_i)} \mathcal{F}_{i,k}^{\text{ex}}, \end{aligned} \tag{3.11}$$

where

$$\mathcal{F}_{i,k}^{\text{ex}} = \int_{\tilde{C}_i \cap C_k} \rho(\mathbf{r}) dV - \int_{C_i \cap \tilde{C}_k} \rho(\mathbf{r}) dV \tag{3.12}$$

are *generalized mass fluxes*. We note that the second cell indicated by the index k may be any cell in the neighborhood and is not restricted to those with whom the cell C_i has a common side. Eq. (3.11) is exact,

and illustrates that the mass of the new cell can be written as the mass of the corresponding old cell plus the exchange of masses with the neighboring cells.

The form above has the important theoretical advantage that it is conservative without requiring any properties in the reconstruction nor an exact integration of the reconstructed function. In fact, any formula of the form

$$m_i^* = m_i + \sum_{k \in \mathcal{C}'(C_i)} \mathcal{F}_{i,k}^*, \tag{3.13}$$

where $\mathcal{F}_{i,k}^* = -\mathcal{F}_{k,i}^*$ some approximation of the flux, will be conservative because of detailed balance. In this form, it is possible to make simplifying approximations that will allow us to avoid the detailed calculation of the intersections between the cells of the new and old meshes without sacrificing exact conservation.

Before proceeding to discuss simplifications, we note that by defining

$$\mathcal{F}_{i,k}^{de} = \rho_k \cdot V(\tilde{C}_i \cap C_k) - \rho_i \cdot V(C_i \cap \tilde{C}_k), \tag{3.14}$$

we recover the CIB/DC defined in (3.4). The associated flux form of the CIB/DC method for the mean density is

$$\rho_i^{de} = \left\{ \frac{1}{V(\tilde{C}_i)} \cdot \left(V(C_i) - \sum_{k \in \mathcal{C}'(C_i)} V(C_i \cap \tilde{C}_k) \right) \right\} \cdot \rho_i + \sum_{k \in \mathcal{C}'(C_i)} \rho_k \cdot \frac{V(\tilde{C}_i \cap C_k)}{V(\tilde{C}_i)}, \tag{3.15}$$

which is equivalent to (3.5). The coefficient of ρ_i is nonnegative; in the worst case C_i does not intersect \tilde{C}_i (i.e., the two cells have no points in common), and \tilde{C}_i is covered-by old cells from $\mathcal{C}'(C_i)$. Then this coefficient is exactly zero. Algorithms based on (3.13) will always be conservative. However, positivity preservation and stability must be investigated for each particular choice of flux.

To implement CIB methods, one has to solve the purely geometric problem of finding cell intersections. This is difficult even in 2D because of geometrical degeneracies, which often occur when the old and new grids are close (as it is the case for ALE methods where rezoning is done on each time step). In 3D further difficulties arise, because the faces of the cells are not planar (see for example, [13]). In the following section, we will describe accurate approximations that do not require finding cell intersections.

4. Simplified face-based donor-cell method

In this section, we describe an approximate remapping method based on the flux form (3.11). We term this the *simplified face-based donor-cell* (SFB/DC) method. The acronym SFB indicates that the method does not require finding intersections between cells on the old and the new meshes. The approximations that we use are based on two ideas. First, up to fourth-order accuracy, the exact masses of new cells can be represented as line integrals of polynomial functions over boundary of a new cell. Second, the line integral over the boundary of the new cell is the line integral over the boundary of the old cell (which is the old mass) plus the line integrals over the regions swept by the movement of the faces (i.e., sides) of the cell C_i .

Here we develop the ideas of the SFB/DC method for a logically rectangular grid (some details for unstructured grids are given in [24]). For logically rectangular grids we adopt the following notation. Vertices (points) are enumerated with two indices $P_{i,j}$: $i = 1, \dots, m$; $j = 1, \dots, n$. Each grid point $P_{i,j}$ has coordinates $(x_{i,j}, y_{i,j})$. The cells have indices $(i + \frac{1}{2}, j + \frac{1}{2})$, with $i = 1, \dots, m - 1$; $j = 1, \dots, n - 1$. The cell $C_{i+\frac{1}{2},j+\frac{1}{2}}$ has vertices $P_{i,j}, P_{i+1,j}, P_{i+1,j+1}, P_{i,j+1}$. The side connecting points $P_{i,j}$ and $P_{i+1,j}$ is $F_{i+\frac{1}{2},j}$ and the side connecting points $P_{i,j}$ and $P_{i,j+1}$ is $F_{i,j+\frac{1}{2}}$.

4.1. Volume and line integrals

Here we show that, for functions $\rho(x, y)$ that have bounded second derivative, the mass (up to fourth-order in mesh size) can be written as the sum of line integrals of polynomial functions over the boundaries of the new cell. These, in turn, are just the usual one-dimensional integrals of polynomials, because the boundaries are just segments of straight lines whose coordinates x and y satisfy a linear equation.

Consider the Taylor series expansion for $\rho(x, y)$ with origin at the point (x^0, y^0)

$$\rho(x, y) = \rho(x^0, y^0) + \frac{\partial \rho}{\partial x} \Big|_{(x^0, y^0)} \cdot (x - x^0) + \frac{\partial \rho}{\partial y} \Big|_{(x^0, y^0)} \cdot (y - y^0) + O\left((x - x^0)^2, (y - y^0)^2\right). \tag{4.1}$$

Using (4.1) with $(x^0, y^0) \in \tilde{C}_{i+\frac{1}{2}, j+\frac{1}{2}}$ and the definition of mass, we derive

$$\begin{aligned} m_{i+\frac{1}{2}, j+\frac{1}{2}}^{\text{ex}} &= \int_{\tilde{C}_{i+\frac{1}{2}, j+\frac{1}{2}}} \rho(x, y) \, dx \, dy \\ &= \rho(x^0, y^0) \cdot \int_{\tilde{C}_{i+\frac{1}{2}, j+\frac{1}{2}}} dx \, dy + \frac{\partial \rho}{\partial x} \Big|_{(x^0, y^0)} \cdot \int_{\tilde{C}_{i+\frac{1}{2}, j+\frac{1}{2}}} (x - x^0) \, dx \, dy \\ &\quad + \frac{\partial \rho}{\partial y} \Big|_{(x^0, y^0)} \cdot \int_{\tilde{C}_{i+\frac{1}{2}, j+\frac{1}{2}}} (y - y^0) \, dx \, dy + O(h^4). \end{aligned} \tag{4.2}$$

Now by Green’s theorem, we have

$$\int_{\tilde{C}_{i+\frac{1}{2}, j+\frac{1}{2}}} dx \, dy = \oint_{\partial \tilde{C}_{i+\frac{1}{2}, j+\frac{1}{2}}} x \, dy, \quad \int_{\tilde{C}_{i+\frac{1}{2}, j+\frac{1}{2}}} x \, dx \, dy = \oint_{\partial \tilde{C}_{i+\frac{1}{2}, j+\frac{1}{2}}} \frac{x^2}{2} \, dy, \quad \int_{\tilde{C}_{i+\frac{1}{2}, j+\frac{1}{2}}} y \, dx \, dy = - \oint_{\partial \tilde{C}_{i+\frac{1}{2}, j+\frac{1}{2}}} \frac{y^2}{2} \, dx,$$

where $\partial \tilde{C}_{i+\frac{1}{2}, j+\frac{1}{2}}$ is the counter-clockwise oriented boundary of the cell $\tilde{C}_{i+\frac{1}{2}, j+\frac{1}{2}}$

$$\partial \tilde{C}_{i+\frac{1}{2}, j+\frac{1}{2}} = \{\tilde{P}_{i,j}, \tilde{P}_{i+1,j}, \tilde{P}_{i+1,j+1}, \tilde{P}_{i,j+1}\}. \tag{4.3}$$

So the computation of the mass of the new cell, up to fourth-order, can be reduced to computation of boundary integrals (assuming that we know the value of ρ and its first derivatives at (x^0, y^0)). Because the cell is a polygon, its boundary is the union of segments of straight lines

$$\partial \tilde{C}_{i+\frac{1}{2}, j+\frac{1}{2}} = \{\tilde{P}_{i,j}, \tilde{P}_{i+1,j}\}; \{\tilde{P}_{i+1,j}, \tilde{P}_{i+1,j+1}\}; \{\tilde{P}_{i+1,j+1}, \tilde{P}_{i,j+1}\}; \{\tilde{P}_{i,j+1}, \tilde{P}_{i,j}\}. \tag{4.4}$$

Now consider

$$\int_{\{\tilde{P}_{i,j}, \tilde{P}_{i+1,j}\}} x \, dy.$$

The equation of the straight line passing through the nodes $\tilde{P}_{i,j}, \tilde{P}_{i+1,j}$ is

$$y = \tilde{y}_{i,j} + \frac{\tilde{y}_{i+1,j} - \tilde{y}_{i,j}}{\tilde{x}_{i+1,j} - \tilde{x}_{i,j}} \cdot (x - \tilde{x}_{i,j}).$$

Thus, on this segment

$$dy = \frac{\tilde{y}_{i+1,j} - \tilde{y}_{i,j}}{\tilde{x}_{i+1,j} - \tilde{x}_{i,j}} \, dx$$

and

$$\int_{\{\tilde{P}_{i,j}, \tilde{P}_{i+1,j}\}} x dy = \frac{\tilde{y}_{i+1,j} - \tilde{y}_{i,j}}{\tilde{x}_{i+1,j} - \tilde{x}_{i,j}} \cdot \int_{\tilde{x}_{i,j}}^{\tilde{x}_{i+1,j}} x dx = \frac{\tilde{y}_{i+1,j} - \tilde{y}_{i,j}}{\tilde{x}_{i+1,j} - \tilde{x}_{i,j}} \left(\frac{\tilde{x}_{i+1,j}^2 - \tilde{x}_{i,j}^2}{2} \right) = (\tilde{y}_{i+1,j} - \tilde{y}_{i,j}) \cdot \frac{\tilde{x}_{i+1,j} - \tilde{x}_{i,j}}{2}.$$

Similar considerations show that, in general, the line integral of a polynomial function over a line segment can be reduced to a one-dimensional integral of the polynomial and can be computed analytically. Therefore, all boundary integrals in (4.2) can be computed analytically; we will not write out these explicit expressions.

4.1.1. Geometric considerations

In Fig. 3, we show a particular example of a cell of an old mesh and its nearest neighbors, with the corresponding cell of the new mesh superposed. We next introduce a new framework for remapping, based on the following decomposition of the volume of the new cell (see Fig. 3):

$$\begin{aligned} \{\tilde{P}_{i,j}, \tilde{P}_{i+1,j}, \tilde{P}_{i+1,j+1}, \tilde{P}_{i,j+1}\} &= \{P_{i,j}, P_{i+1,j}, P_{i+1,j+1}, P_{i,j+1}\} + \{P_{i+1,j}, \tilde{P}_{i+1,j}, \tilde{P}_{i+1,j+1}, P_{i+1,j+1}\} \\ &\quad - \{P_{i,j}, \tilde{P}_{i,j}, \tilde{P}_{i,j+1}, P_{i,j+1}\} + \{P_{i,j+1}, P_{i+1,j+1}, \tilde{P}_{i+1,j+1}, \tilde{P}_{i,j+1}\} \\ &\quad - \{P_{i,j}, P_{i+1,j}, \tilde{P}_{i+1,j}, \tilde{P}_{i,j}\}. \end{aligned} \tag{4.5}$$

The first term of the right-hand side of (4.5) is the boundary of the old cell, $C_{i+\frac{1}{2},j+\frac{1}{2}}$. We note that the areas that are covered by the continuous movement of the faces from their old to their new positions, which we term the *swept regions*, can be written as

$$\delta F_{i+\frac{1}{2},j} = \{P_{i,j}, P_{i+1,j}, \tilde{P}_{i+1,j}, \tilde{P}_{i,j}\}, \quad \delta F_{i,j+\frac{1}{2}} = \{P_{i,j}, \tilde{P}_{i,j}, \tilde{P}_{i,j+1}, P_{i,j+1}\},$$

etc. Using this definition, we rewrite (4.5) as

$$\partial(\tilde{C}_{i+\frac{1}{2},j+\frac{1}{2}}) = \partial(C_{i+\frac{1}{2},j+\frac{1}{2}}) + \partial(\delta F_{i+1,j+\frac{1}{2}}) - \partial(\delta F_{i,j+\frac{1}{2}}) + \partial(\delta F_{i+\frac{1}{2},j+1}) - \partial(\delta F_{i+\frac{1}{2},j}). \tag{4.6}$$

This partitioning is valid for other relative locations of old and new meshes as shown in Figs. 4(a) and (b).

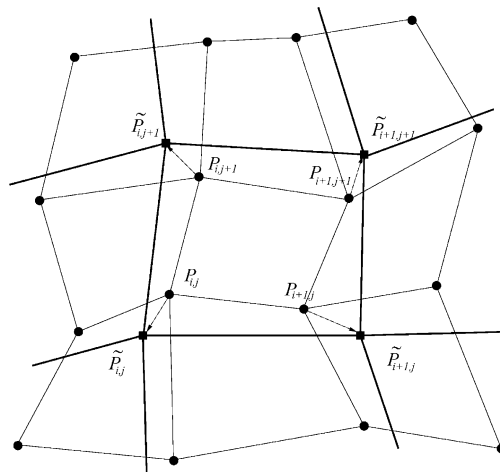


Fig. 3. Old and new mesh. Vertices of the old mesh are marked by solid circles, and vertices of the new mesh are marked by solid squares. Sides of the new mesh are bold lines, and displacements of the vertices are shown by dashed arrows.

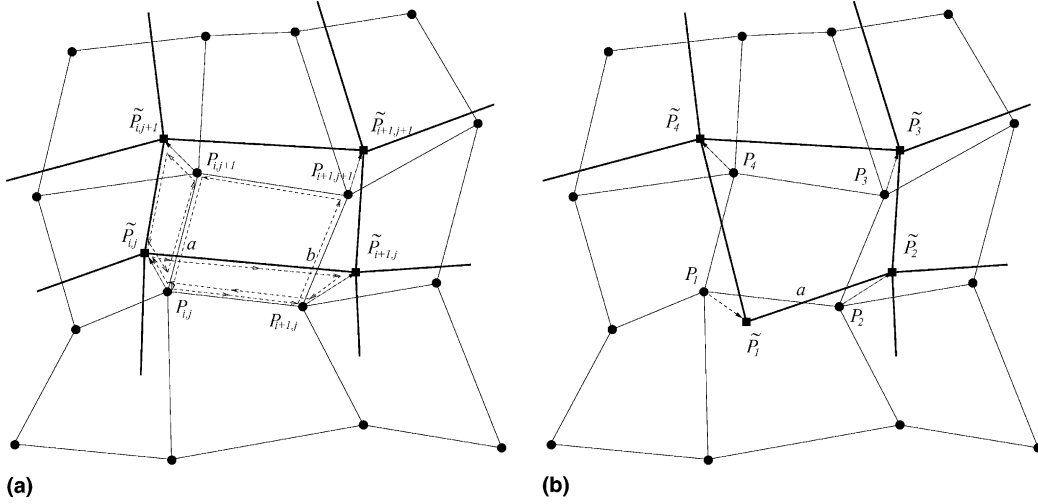


Fig. 4. Partitioning of the new cell into the old cell and the swept regions.

In general, the swept regions can overlap each other. The two line integrals around an overlapped region will cancel because of the opposite orientations of the boundaries. For example, in Fig. 4(a), the triangle $P_{i,j}$, a , $\tilde{P}_{i,j}$ (where a is the intersection of segments $\tilde{P}_{i,j}$, $\tilde{P}_{i+1,j}$ and $P_{i,j}$, $P_{i,j+1}$) is not a part of new cell $\tilde{C}_{i+\frac{1}{2},j+\frac{1}{2}}$, but is part of both of the swept regions $\delta F_{i+\frac{1}{2},j}$ and $\delta F_{i,j+\frac{1}{2}}$. However, the contribution of this triangle to the new cell volume is zero; e.g., the contribution of the segment $aP_{i,j}$ is zero because it participates in both the line integral over the boundary of the old cell, and the line integral over the boundary of the swept region $\delta F_{i,j+\frac{1}{2}}$, with opposite signs. Similarly, the area integrals of density over this triangle in the swept regions $\delta F_{i,j+\frac{1}{2}}$ and $\delta F_{i+\frac{1}{2},j}$ appear with opposite sign and cancel. These cancellations are easily recognized by recalling $\int_{AB} = -\int_{BA}$.

Now the expression for the new cell mass can be written as that of the old cell and plus contributions from the swept regions

$$\oint_{\partial \tilde{C}_{i+\frac{1}{2},j+\frac{1}{2}}} = \oint_{\partial C_{i+\frac{1}{2},j+\frac{1}{2}}} + \oint_{\partial(\delta F_{i+1,j+\frac{1}{2}})} - \oint_{\partial(\delta F_{i,j+\frac{1}{2}})} + \oint_{\partial(\delta F_{i+\frac{1}{2},j+1})} - \oint_{\partial(\delta F_{i+\frac{1}{2},j})},$$

where in each integral the integrand is the density. Since the volume integral and the boundary integrals are equivalent for linear functions, we can write the following compact formula for the new mass:

$$m_{i+\frac{1}{2},j+\frac{1}{2}}^{\text{ex}} = m_{i+\frac{1}{2},j+\frac{1}{2}} + \mathcal{F}_{i+1,j+\frac{1}{2}}^{\text{ex}} - \mathcal{F}_{i,j+\frac{1}{2}}^{\text{ex}} + \mathcal{F}_{i+\frac{1}{2},j+1}^{\text{ex}} - \mathcal{F}_{i+\frac{1}{2},j}^{\text{ex}}, \tag{4.7}$$

where the exact “fluxes” \mathcal{F}_{ex} are

$$\mathcal{F}_{i,j+\frac{1}{2}}^{\text{ex}} = \int_{\partial F_{i,j+\frac{1}{2}}} \left(\rho + \frac{\partial \rho}{\partial x} \cdot (x - x_{i,j+\frac{1}{2}}) + \frac{\partial \rho}{\partial y} \cdot (y - y_{i,j+\frac{1}{2}}) \right) dx dy + O(h^4). \tag{4.8}$$

Here ρ and its derivatives are all evaluated at the point

$$P_{i,j+\frac{1}{2}} = (x_{i,j+\frac{1}{2}}, y_{i,j+\frac{1}{2}}).$$

This equation results from using a Taylor series expansion about the point $P_{i,j+\frac{1}{2}}$. Similarly,

$$\mathcal{F}_{i+\frac{1}{2},j}^{\text{ex}} = \int_{\partial F_{i+\frac{1}{2},j}} \left(\rho + \frac{\partial \rho}{\partial x} \cdot (x - x_{i+\frac{1}{2},j}) + \frac{\partial \rho}{\partial y} \cdot (y - y_{i+\frac{1}{2},j}) \right) dx dy + O(h^4), \tag{4.9}$$

where ρ and its derivatives are evaluated at

$$P_{i+\frac{1}{2},j} = (x_{i+\frac{1}{2},j}, y_{i+\frac{1}{2},j}).$$

4.2. SFB/DC method

Now consider the situation presented in Fig. 5(a), where just one vertex, $P_{i,j}$ has been moved to a new position $\tilde{P}_{i,j}$. Application of the flux version of the CIB/DC method (3.15) to this particular case gives

$$m_{i+\frac{1}{2},j+\frac{1}{2}}^{\text{dc}} = m_{i+\frac{1}{2},j+\frac{1}{2}} + \rho_{i-\frac{1}{2},j+\frac{1}{2}} \cdot V_{a,P_{i,j},\tilde{P}_{i,j+1}} + \rho_{i-\frac{1}{2},j-\frac{1}{2}} \cdot V_{a,\tilde{P}_{i,j},b,P_{i,j}} + \rho_{i+\frac{1}{2},j-\frac{1}{2}} \cdot V_{b,P_{i+1,j},P_{i,j}}, \tag{4.10}$$

where V is the positive volume defined by its subscripts. Here a and b are the intersections of the sides of the new and old cells, see Fig. 5(a).

The line segment $\{P_{i,j}, \tilde{P}_{i,j}\}$ divides the quadrilateral $\{a, \tilde{P}_{i,j}, b, P_{i,j}\}$ into two triangles $\{a, \tilde{P}_{i,j}, P_{i,j}\}$ and $\{\tilde{P}_{i,j}, b, P_{i,j}\}$. Now it is easy to see that the union of the triangle $\{a, \tilde{P}_{i,j}, P_{i,j}\}$ with the triangle

$$\{a, P_{i,j}, \tilde{P}_{i,j+1}\} = \tilde{C}_{i+\frac{1}{2},j+\frac{1}{2}} \cap C_{i-\frac{1}{2},j+\frac{1}{2}}$$

is the swept region $\delta F_{i,j+\frac{1}{2}}$. Similarly, the union of the triangle $\{\tilde{P}_{i,j}, b, P_{i,j}\}$ and the triangle $\{\tilde{P}_{i+1,j}, b, P_{i,j}\} = \tilde{C}_{i+\frac{1}{2},j+\frac{1}{2}} \cap C_{i+\frac{1}{2},j-\frac{1}{2}}$ is the swept region $\delta F_{i+\frac{1}{2},j}$. Thus (4.10) can be rewritten

$$m_{i+\frac{1}{2},j+\frac{1}{2}}^{\text{dc}} = m_{i+\frac{1}{2},j+\frac{1}{2}} - \rho_{i-\frac{1}{2},j+\frac{1}{2}} \cdot V(\delta F_{i,j+\frac{1}{2}}) - \rho_{i+\frac{1}{2},j-\frac{1}{2}} \cdot V(\delta F_{i+\frac{1}{2},j}) + \left\{ (\rho_{i-\frac{1}{2},j-\frac{1}{2}} - \rho_{i+\frac{1}{2},j-\frac{1}{2}}) \cdot V_{\tilde{P}_{i,j},b,P_{i,j}} + (\rho_{i-\frac{1}{2},j-\frac{1}{2}} - \rho_{i-\frac{1}{2},j+\frac{1}{2}}) \cdot V_{a,\tilde{P}_{i,j},P_{i,j}} \right\}, \tag{4.11}$$

where the volumes of the swept regions are negative due to the sign convention adopted in the previous section. It is clear that the second and third terms on the right-hand-side of (4.11) are piecewise constant

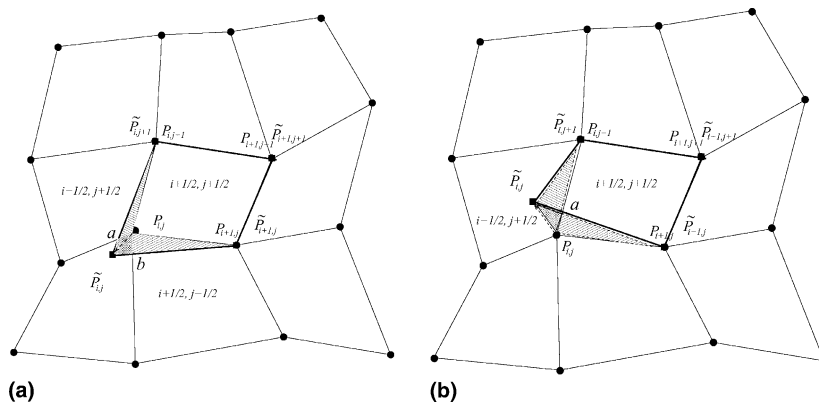


Fig. 5. Comparison of CIB/DC and SFB/DC.

approximations to the corresponding fluxes in (4.7). The expression in curly brackets on the second line of (4.11) is $O(h^3)$ for smooth functions $\rho(\mathbf{r})$. Thus, if we define $m_{i+\frac{1}{2},j+\frac{1}{2}}^{\text{da}}$ as

$$m_{i+\frac{1}{2},j+\frac{1}{2}}^{\text{da}} = m_{i+\frac{1}{2},j+\frac{1}{2}} - \rho_{i-1/2,j+\frac{1}{2}} \cdot V(\delta F_{i,j+\frac{1}{2}}) - \rho_{i+\frac{1}{2},j-\frac{1}{2}} \cdot V(\delta F_{i+\frac{1}{2},j}), \quad (4.12)$$

then

$$m_{i+\frac{1}{2},j+\frac{1}{2}}^{\text{da}} - m_{i+\frac{1}{2},j+\frac{1}{2}}^{\text{dc}} = O(h^3).$$

That is, the formal order of accuracy of $m_{i+\frac{1}{2},j+\frac{1}{2}}^{\text{da}}$ with respect to the exact mass is the same as the order of accuracy of the CIB/DC method.

In the situation depicted in Fig. 5(b)

$$m_{i+\frac{1}{2},j+\frac{1}{2}}^{\text{dc}} = m_{i+\frac{1}{2},j+\frac{1}{2}} + \rho_{i-\frac{1}{2},j+\frac{1}{2}} \cdot V_{a,\tilde{P}_{i,j},\tilde{P}_{i,j+1}} - \rho_{i+\frac{1}{2},j-\frac{1}{2}} \cdot V_{a,P_{i,j},P_{i+1,j}}. \quad (4.13)$$

Using similar arguments as presented for the case depicted in Fig. 5(a), we have

$$m_{i+\frac{1}{2},j+\frac{1}{2}}^{\text{dc}} = m_{i+\frac{1}{2},j+\frac{1}{2}} - \rho_{i-1/2,j+\frac{1}{2}} \cdot V(\delta F_{i,j+\frac{1}{2}}) - \rho_{i+\frac{1}{2},j+\frac{1}{2}} \cdot V(\delta F_{i+\frac{1}{2},j}) + \left\{ (\rho_{i-\frac{1}{2},j+\frac{1}{2}} - \rho_{i+\frac{1}{2},j+\frac{1}{2}}) \cdot V_{\tilde{P}_{i,j},P_{i,j},a} \right\}, \quad (4.14)$$

where the volume of the swept region $\delta F_{i,j+\frac{1}{2}}$ is negative, but volume of $\delta F_{i+\frac{1}{2},j}$ is now positive. Note that the density in the term on the right-hand-side now is that of cell $C_{i+\frac{1}{2},j+\frac{1}{2}}$. The error in this approximation is again $O(h^3)$, since the triangle $\{\tilde{P}_{i,j}, P_{i,j}, a\}$ appears in both swept regions, but with opposite sign, and so cancels. Thus, if we define the approximate mass as

$$m_{i+\frac{1}{2},j+\frac{1}{2}}^{\text{da}} = m_{i+\frac{1}{2},j+\frac{1}{2}} - \rho_{i-1/2,j+\frac{1}{2}} \cdot V(\delta F_{i,j+\frac{1}{2}}) - \rho_{i+\frac{1}{2},j+\frac{1}{2}} \cdot V(\delta F_{i+\frac{1}{2},j}), \quad (4.15)$$

we maintain the same formal order of accuracy as the original CIB/DC has.

Based on the previous examples, we now define a new simplified face-based donor-cell (SFB/DC) as follows:

$$m_{i+\frac{1}{2},j+\frac{1}{2}}^{\text{da}} = m_{i+\frac{1}{2},j+\frac{1}{2}} + \mathcal{F}_{i+1,j+\frac{1}{2}}^{\text{da}} - \mathcal{F}_{i,j+\frac{1}{2}}^{\text{da}} + \mathcal{F}_{i+\frac{1}{2},j+1}^{\text{da}} - \mathcal{F}_{i+\frac{1}{2},j}^{\text{da}}. \quad (4.16)$$

Here the approximate “fluxes” are

$$\mathcal{F}_{i,j+\frac{1}{2}}^{\text{da}} = \rho_{i,j+\frac{1}{2}} \cdot V(\delta F_{i,j+\frac{1}{2}}), \quad \mathcal{F}_{i+\frac{1}{2},j}^{\text{da}} = \rho_{i+\frac{1}{2},j} \cdot V(\delta F_{i+\frac{1}{2},j}), \quad (4.17)$$

etc., and where $V(\delta F_{i,j+\frac{1}{2}})$ is a signed volume. The density on the faces depends on the sign of the volume of the swept region (as appeared in the examples at the beginning of this section):

$$\rho_{i,j+\frac{1}{2}} = \begin{cases} \rho_{i+\frac{1}{2},j+\frac{1}{2}}, & V(\delta F_{i,j+\frac{1}{2}}) \geq 0, \\ \rho_{i-\frac{1}{2},j+\frac{1}{2}}, & V(\delta F_{i,j+\frac{1}{2}}) < 0, \end{cases} \quad \rho_{i+\frac{1}{2},j} = \begin{cases} \rho_{i+\frac{1}{2},j+\frac{1}{2}}, & V(\delta F_{i+\frac{1}{2},j}) \geq 0, \\ \rho_{i+\frac{1}{2},j-\frac{1}{2}}, & V(\delta F_{i+\frac{1}{2},j}) < 0. \end{cases} \quad (4.18)$$

Because the SFB/DC is not equivalent to CIB/DC, there is no guarantee that mean density over new cell will always be a positive combination of the old densities. First, let us analyze the formulas (4.16)–(4.18) from this point of view for the example presented in Fig. 5. The expression for the new mass in the SFB/DC method is defined in (4.15), which can be rewritten in terms of densities as follows:

$$\rho_{i+\frac{1}{2},j+\frac{1}{2}}^{\text{da}} = \frac{1}{V(\tilde{C}_{i+\frac{1}{2},j+\frac{1}{2}})} \cdot \left\{ V(C_{i+\frac{1}{2},j+\frac{1}{2}}) - \left| V(\delta F_{i+\frac{1}{2},j}) \right| \right\} \cdot \rho_{i+\frac{1}{2},j+\frac{1}{2}} + \left| V(\delta F_{i,j+\frac{1}{2}}) \right| \cdot \rho_{i-1/2,j+\frac{1}{2}}. \quad (4.19)$$

A sufficient condition for positivity of density is

$$\left| V(\delta F_{i+\frac{1}{2},j}) \right| \leq V(C_{i+\frac{1}{2},j+\frac{1}{2}}). \quad (4.20)$$

The necessary condition may be much weaker due to any positive contribution from the cell $C_{i-\frac{1}{2},j+\frac{1}{2}}$, see (4.14). However, the condition (4.20) may become necessary if

$$\rho_{i-\frac{1}{2},j+\frac{1}{2}} \ll \rho_{i+\frac{1}{2},j+\frac{1}{2}}.$$

More generally, we can write the SFB/DC method in terms of densities as follows:

$$\begin{aligned} \rho_{i+\frac{1}{2},j+\frac{1}{2}}^{\text{da}} = & \frac{1}{V(\tilde{C}_{i+\frac{1}{2},j+\frac{1}{2}})} \left\{ V(C_{i+\frac{1}{2},j+\frac{1}{2}}) \right. \\ & + \frac{V(\delta F_{i+1,j+\frac{1}{2}}) - \left| V(\delta F_{i+1,j+\frac{1}{2}}) \right|}{2} - \frac{V(\delta F_{i,j+\frac{1}{2}}) + \left| V(\delta F_{i,j+\frac{1}{2}}) \right|}{2} \\ & + \frac{V(\delta F_{i+1,j+\frac{1}{2}}) - \left| V(\delta F_{i+1,j+\frac{1}{2}}) \right|}{2} - \frac{V(\delta F_{i,j+\frac{1}{2}}) + \left| V(\delta F_{i,j+\frac{1}{2}}) \right|}{2} \left. \right\} \cdot \rho_{i+\frac{1}{2},j+\frac{1}{2}} \\ & + \frac{V(\delta F_{i+1,j+\frac{1}{2}}) + \left| V(\delta F_{i+1,j+\frac{1}{2}}) \right|}{2} \cdot \rho_{i+\frac{3}{2},j+\frac{1}{2}} - \frac{V(\delta F_{i,j+\frac{1}{2}}) - \left| V(\delta F_{i,j+\frac{1}{2}}) \right|}{2} \cdot \rho_{i-\frac{1}{2},j+\frac{1}{2}} \\ & + \frac{V(\delta F_{i+\frac{1}{2},j+1}) + \left| V(\delta F_{i+\frac{1}{2},j+1}) \right|}{2} \cdot \rho_{i+\frac{1}{2},j+\frac{3}{2}} - \frac{V(\delta F_{i+\frac{1}{2},j}) - \left| V(\delta F_{i+\frac{1}{2},j}) \right|}{2} \cdot \rho_{i+\frac{1}{2},j-\frac{1}{2}}. \quad (4.21) \end{aligned}$$

In this complicated expression, the coefficients of all the density terms are positive or zero, excepting possibly that of the central density $\rho_{i+\frac{1}{2},j+\frac{1}{2}}$. For the central density coefficient to be positive, we will have to impose additional restrictions on the displacements that guarantee that the sum of all the negatively signed volumes (those taken from the volume of the original cell) of the swept regions do not exceed $V(C_{i+\frac{1}{2},j+\frac{1}{2}})$.

An important property of the SFB/DC method is that positivity (and, therefore the boundness of the new densities) depends only on the displacement field.

Although CIB/DC and SFB/DC have the same order of accuracy for smooth $\rho(\mathbf{r})$ – i.e., they both are first-order accurate – we have not yet discussed the case of nonsmooth $\rho(\mathbf{r})$. This will be illustrated in numerical examples. We close this section by remarking that while we are not actually interested in first-order methods, we will use the same framework to construct second-order methods.

5. Positivity-preserving error compensation algorithm

In this section, we analyze the errors related to the SFB/DC method and describe a technique that compensates these errors, leading to a second-order accurate method that preserves the positivity property

of SFB/DC. This compensation was inspired by multidimensional positive definite advection transport algorithm (MPDATA), which underlies several nonoscillatory advection schemes; see [21,31,32].

5.1. 1D error analysis and compensation

Consider a nonuniform 1D *old* grid whose nodal coordinates are contained in the interval $[x_{\min}, x_{\max}]$: $x_{\min} = x_1 < x_2, \dots, x_{m-1} < x_m = x_{\max}$. The cells of the grid are labeled by half indices $-C_{i+\frac{1}{2}}$. The coordinate of the cell center is $x_{i+\frac{1}{2}} = (x_{i+1} + x_i)/2$, and the length of the cell is $h_{i+\frac{1}{2}} = V(C_{i+\frac{1}{2}}) = x_{i+1} - x_i$. Coordinates of the new grid are distinguished with a “tilde”, e.g., \tilde{x}_i , etc. The exact mass of a new cell is

$$m_{i+\frac{1}{2}}^{\text{ex}} = \int_{\tilde{x}_i}^{\tilde{x}_{i+1}} \rho(x) dx = \int_{\tilde{x}_i}^{x_i} \rho(x) dx + \int_{x_i}^{x_{i+1}} \rho(x) dx + \int_{x_{i+1}}^{\tilde{x}_{i+1}} \rho(x) dx, \tag{5.1}$$

which is valid for either $\tilde{x}_i \geq x_i$ or $\tilde{x}_i \leq x_i$.

The flux form of (5.1) is written

$$m_{i+\frac{1}{2}}^{\text{ex}} = m_{i+\frac{1}{2}} + \mathcal{F}_{i+1}^{\text{ex}} - \mathcal{F}_i^{\text{ex}}, \tag{5.2}$$

where

$$\mathcal{F}_i^{\text{ex}} = \int_{x_i}^{\tilde{x}_i} \rho(x) dx \tag{5.3}$$

is the exact density flux at node i . In the 1D case, the swept region for $F_i = x_i$ is $\delta F_i = [\tilde{x}_i, x_i]$.

The SFB/DC algorithm in 1D is

$$m_{i+\frac{1}{2}}^{\text{da}} = m_{i+\frac{1}{2}} + \mathcal{F}_{i+1}^{\text{da}} - \mathcal{F}_i^{\text{da}}. \tag{5.4}$$

Let the displacement of the i -th node be $\delta x_i = V(\delta F_i) = \tilde{x}_i - x_i$. Then $\mathcal{F}_i^{\text{da}}$ is defined as

$$\mathcal{F}_i^{\text{da}} = \rho_i \cdot \delta x_i, \tag{5.5}$$

where

$$\rho_i = \begin{cases} \rho_{i+\frac{1}{2}}, & \delta x_i \geq 0, \\ \rho_{i-\frac{1}{2}}, & \delta x_i < 0. \end{cases} \tag{5.6}$$

The error of the donor-cell approximation in 1D for mass is

$$m_{i+\frac{1}{2}}^{\text{ex}} - m_{i+\frac{1}{2}}^{\text{da}} = e_{i+1}^{\text{ex}} - e_i^{\text{ex}}, \tag{5.7}$$

where e_i^{ex} , the error in the density flux at node i , is

$$e_i^{\text{ex}} = \mathcal{F}_i^{\text{ex}} - \mathcal{F}_i^{\text{da}} = \begin{cases} \int_{x_i}^{x_i+\delta x_i} \rho dx - \delta x_i \cdot \rho_{i+\frac{1}{2}}, & \delta x_i \geq 0, \\ \int_{x_i}^{x_i+\delta x_i} \rho dx - \delta x_i \cdot \rho_{i-\frac{1}{2}}, & \delta x_i < 0, \end{cases} \tag{5.8}$$

To estimate this error, we use the Taylor expansion of the function $\rho(x)$ at the cell center $x_{i+\frac{1}{2}}$ if $\delta x_i > 0$, or at the cell center $x_{i-\frac{1}{2}}$ if $\delta x_i < 0$. If $\delta x_i > 0$, then

$$\rho(x) = \rho(x_{i+\frac{1}{2}}) + \left. \frac{d\rho}{dx} \right|_{x_{i+\frac{1}{2}}} \cdot (x - x_{i+\frac{1}{2}}) + O(h^2) = \rho_{i+\frac{1}{2}} + \left. \frac{d\rho}{dx} \right|_{x_{i+\frac{1}{2}}} \cdot (x - x_{i+\frac{1}{2}}) + O(h^2), \tag{5.9}$$

because $\rho(x_{i+\frac{1}{2}}) = \rho_{i+\frac{1}{2}} + O(h^2)$.

Using the Taylor expansion (5.9) or the similar expansion about $x_{i-\frac{1}{2}}$, we can rewrite the error in (5.8) as

$$e_i^{\text{ex}} = \begin{cases} \frac{d\rho}{dx} \Big|_{x_{i+\frac{1}{2}}} \cdot \int_{x_i}^{\bar{x}_i} (x - x_{i+\frac{1}{2}}) dx + O(h^3), & \delta x_i \geq 0, \\ \frac{d\rho}{dx} \Big|_{x_{i-\frac{1}{2}}} \cdot \int_{x_i}^{\bar{x}_i} (x - x_{i-\frac{1}{2}}) dx + O(h^3), & \delta x_i < 0. \end{cases} \tag{5.10}$$

The integrals can be computed explicitly, yielding

$$e_i^{\text{ex}} = \begin{cases} \frac{\delta x_i}{2} \cdot \frac{d\rho}{dx} \Big|_{x_{i+\frac{1}{2}}} \cdot (\delta x_i - h_{i+\frac{1}{2}}) + O(h^3), & \delta x_i \geq 0, \\ \frac{\delta x_i}{2} \cdot \frac{d\rho}{dx} \Big|_{x_{i-\frac{1}{2}}} \cdot (\delta x_i + h_{i-\frac{1}{2}}) + O(h^3), & \delta x_i < 0. \end{cases} \tag{5.11}$$

The error e_i^{ex} in the mass is $O(h^2)$: since density is mass/length, and length is $O(h)$; i.e., the error in density is first order.

Suppose that we have a first-order approximation for $d\rho/dx$:

$$\left(\frac{\delta\rho}{\delta x} \right)_{i\pm\frac{1}{2}} = \frac{d\rho}{dx} \Big|_{x_{i\pm\frac{1}{2}}} + O(h). \tag{5.12}$$

Dropping all terms of $O(h^3)$, we derive the following estimate for the error in the flux:

$$e_i^* = \begin{cases} \frac{\delta x_i}{2} \cdot \left(\frac{\delta\rho}{\delta x} \right)_{i+\frac{1}{2}} \cdot (\delta x_i - h_{i+\frac{1}{2}}), & \delta x_i \geq 0, \\ \frac{\delta x_i}{2} \cdot \left(\frac{\delta\rho}{\delta x} \right)_{i-\frac{1}{2}} \cdot (\delta x_i + h_{i-\frac{1}{2}}), & \delta x_i < 0 \end{cases} \tag{5.13}$$

to $O(h^3)$.

We can use this estimate to compensate the error and so improve the order of accuracy of the remap. Specifically, we can obtain a third-order accurate approximation for $m_{i+\frac{1}{2}}$, in contrast to the donor-cell approximation, which is second-order accurate, by approximately compensating the error in fluxes:

$$m_{i+\frac{1}{2}}^{\text{ex}} \approx m_{i+\frac{1}{2}}^{\text{da}} + e_{i+1}^* - e_i^*. \tag{5.14}$$

The important issue at this point is how to approximate the density derivative $(\delta\rho/\delta x)_{i+\frac{1}{2}}$. When $\rho(\mathbf{r})$ is smooth, the choice of $(\delta\rho/\delta x)_{i+\frac{1}{2}}$ may affect the monotonicity of the remap, but probably will not have any other significant effect. When $\rho(\mathbf{r})$ is not smooth, the properties of the remapping algorithm may depend significantly on this choice.

The simplest approximation is the central differencing

$$\left(\frac{\delta\rho}{\delta x} \right)_{i+\frac{1}{2}} = \frac{\rho_{i+\frac{1}{2}} - \rho_{i-\frac{1}{2}}}{x_{i+\frac{1}{2}} - x_{i-\frac{1}{2}}} = \frac{\rho_{i+\frac{1}{2}} - \rho_{i-\frac{1}{2}}}{0.5 \cdot (h_{i+\frac{1}{2}} + h_{i-\frac{1}{2}})}. \tag{5.15}$$

This choice is easily recognized as being equivalent to linear reconstruction of the density between cell centers, and leads to the following error estimate:

$$e_i^{\text{center}} = \begin{cases} \frac{\delta x_i}{2} \cdot \frac{\rho_{i+\frac{1}{2}} - \rho_{i-\frac{1}{2}}}{0.5 \cdot (h_{i+\frac{1}{2}} + h_{i-\frac{1}{2}})} \cdot (\delta x_i - h_{i+\frac{1}{2}}), & \delta x_i \geq 0, \\ \frac{\delta x_i}{2} \cdot \frac{\rho_{i+\frac{1}{2}} - \rho_{i-\frac{1}{2}}}{0.5 \cdot (h_{i+\frac{1}{2}} + h_{i-\frac{1}{2}})} \cdot (\delta x_i + h_{i-\frac{1}{2}}), & \delta x_i < 0. \end{cases} \tag{5.16}$$

However, it is well known that central differencing, used directly in (5.14), can produce negative ρ (i.e., the algorithm is not positivity preserving) and in many circumstances may be computationally unstable.

Instead, we have chosen to proceed in the spirit of [31] compensating the error with an approximation of e_i^{center} that depends on the sign of the displacement. The resulting algorithm will always produce a positive density with suitable restrictions on the grid movement. We use the superscript mc for this approximation. The equations have the form

$$m_{i+\frac{1}{2}}^{\text{mc}} = m_{i+\frac{1}{2}}^{\text{da}} + \mathcal{F}_{i+1}^{\text{mc}} - \mathcal{F}_i^{\text{mc}}, \tag{5.17}$$

where the corrective fluxes \mathcal{F}^{mc} are defined as

$$\mathcal{F}_i^{\text{mc}} = \frac{\rho_i^{\text{da}}}{0.5(\rho_{i+\frac{1}{2}} + \rho_{i-\frac{1}{2}})} \cdot e_i^{\text{center}} \tag{5.18}$$

and

$$\rho_i^{\text{da}} = \begin{cases} \rho_{i+\frac{1}{2}}^{\text{da}}, & e_i^{\text{center}} \geq 0, \\ \rho_{i-\frac{1}{2}}^{\text{da}}, & e_i^{\text{center}} < 0. \end{cases} \tag{5.19}$$

There are alternative methods to estimate $(\delta\rho/\delta x)_{i+\frac{1}{2}}$ in the error (5.13). In [24] we consider one such method, based on the *minmod* procedure of estimating derivatives, see e.g., [18]. A formal analysis shows that the minmod derivative is first-order accurate, as is required in our derivations. We will call this the mm method. In [24] we demonstrated with numerical examples that the minmod approach can significantly improve the preservation of monotonicity when compared with the original mc method, while imposing less restriction on the displacement field. However, mm produces less sharp profiles than the mc method.

To investigate the accuracy of the mc remapping, we assume that $\rho(x)$ is a smooth function of x . We make *no* assumptions about the smoothness of the grid or the displacements δx_i . We note that $e_i^{\text{center}} = O(h^2)$. Further, the coefficient of e_i^{center} in (5.18) is equal to $1 + O(h)$. Thus we have

$$\mathcal{F}_i^{\text{mc}} = (1 + O(h)) \cdot e_i^{\text{center}} = e_i^{\text{ex}} + O(h^3)$$

and so the mc remapping method is third-order accurate for mass.

To interpret formulas (5.17)–(5.19), it is convenient to define pseudo displacements by

$$\Delta x_i = \frac{e_i^{\text{center}}}{0.5(\rho_{i+\frac{1}{2}} + \rho_{i-\frac{1}{2}})}, \tag{5.20}$$

noting that e_i^{center} has the same sign as Δx_i . Now the fluxes in the mc method, (5.18) and (5.19), can be written in a form that resembles those for the donor-cell method, (5.5) and (5.6):

$$\mathcal{F}_i^{\text{mc}} = \rho_i^{\text{da}} \cdot \Delta x_i, \tag{5.21}$$

where

$$\rho_i^{\text{da}} = \begin{cases} \rho_{i+\frac{1}{2}}^{\text{da}}, & \Delta x_i \geq 0, \\ \rho_{i-\frac{1}{2}}^{\text{da}}, & \Delta x_i < 0. \end{cases} \tag{5.22}$$

To illustrate the remapping based on (5.17), assume that Δx_i and Δx_{i+1} are positive. Then

$$m_{i+\frac{1}{2}}^{\text{mc}} = m_{i+\frac{1}{2}}^{\text{da}} + \rho_{i+\frac{3}{2}}^{\text{da}} \cdot \Delta x_{i+1} - \rho_{i+\frac{1}{2}}^{\text{da}} \cdot \Delta x_i \tag{5.23}$$

and

$$\rho_{i+\frac{1}{2}}^{mc} = \left(\frac{\tilde{h}_{i+\frac{1}{2}} - \Delta x_i}{\tilde{h}_{i+\frac{1}{2}}} \right) \rho_{i+\frac{1}{2}}^{da} + \left(\frac{\Delta x_{i+1}}{\tilde{h}_{i+\frac{3}{2}}} \right) \rho_{i+\frac{3}{2}}^{da}. \tag{5.24}$$

The coefficient of $\rho_{i+\frac{3}{2}}^{da}$ is positive by assumption. For the coefficient of $\rho_{i+\frac{1}{2}}^{da}$ to be positive, we must require

$$\Delta x_i < \tilde{h}_{i+\frac{1}{2}}.$$

More generally, the positivity will depend on the displacements at both sides of the cell. To allow for pseudo displacements at both vertices, it is sufficient to require

$$\Delta x_i < \frac{h_{i+\frac{1}{2}}}{2}. \tag{5.25}$$

An important difference between the da and mc methods is that the sum of coefficients is not equal to unity in the latter case. The sum of coefficients is actually

$$\frac{\tilde{h}_{i+\frac{1}{2}} - \Delta x_i + \Delta x_{i+1}}{\tilde{h}_{i+\frac{1}{2}}} = 1 + \frac{\Delta x_{i+1} - \Delta x_i}{\tilde{h}_{i+\frac{1}{2}}}. \tag{5.26}$$

In general, the discrepancy

$$r = \frac{\Delta x_{i+1} - \Delta x_i}{\tilde{h}_{i+\frac{1}{2}}} \tag{5.27}$$

will be nonzero, of either sign, and have magnitude up to 1. However, enforcing the positivity of density will require us to restrict the rezone displacement. Using (5.20) and (5.13), we can write:

$$\Delta x_i = \delta x_i \cdot \frac{\rho_{i+\frac{1}{2}} - \rho_{i-\frac{1}{2}}}{\rho_{i+\frac{1}{2}} + \rho_{i-\frac{1}{2}}} \cdot \frac{\delta x_i - h_{i+\frac{1}{2}}}{0.5(\tilde{h}_{i+\frac{1}{2}} + \tilde{h}_{i-\frac{1}{2}})}. \tag{5.28}$$

Assume that the displacement δx_i is positive; then the first factor in (5.28) is positive, and the third factor is negative. However the second factor can be of either sign. The more restrictive case, in the sense of satisfying (5.25) occurs when

$$\rho_{i+\frac{1}{2}} < \rho_{i-\frac{1}{2}}.$$

Then the second factor is negative and Δx_i is positive.

Since ρ is positive,

$$\left| \frac{\rho_{i+\frac{1}{2}} - \rho_{i-\frac{1}{2}}}{\rho_{i+\frac{1}{2}} + \rho_{i-\frac{1}{2}}} \right| \leq 1. \tag{5.29}$$

However this ratio can be very close to 1 if $\rho_{i+\frac{1}{2}} \ll \rho_{i-\frac{1}{2}}$ or vice versa. Thus, as a sufficient condition, (5.28) can be written

$$\Delta x_i \leq \delta x_i \cdot \frac{h_{i+\frac{1}{2}} - \delta x_i}{0.5(\tilde{h}_{i+\frac{1}{2}} + \tilde{h}_{i-\frac{1}{2}})}. \tag{5.30}$$

Expressing $\tilde{h}_{i+\frac{1}{2}}$ and $\tilde{h}_{i-\frac{1}{2}}$ in terms of $h_{i+\frac{1}{2}}$ and $h_{i-\frac{1}{2}}$, we can write

$$\frac{h_{i+\frac{1}{2}} - \delta x_i}{0.5(\tilde{h}_{i+\frac{1}{2}} + \tilde{h}_{i-\frac{1}{2}})} = \frac{h_{i+\frac{1}{2}} - \delta x_i}{0.5(h_{i+\frac{1}{2}} + h_{i-\frac{1}{2}} + \delta x_{i+1} - \delta x_{i-1})}.$$

In the worse case.

$$h_{i-\frac{1}{2}} \approx 0, \quad \delta x_i \approx 0 \approx \delta x_{i+1}, \quad \delta x_{i-1} \approx \frac{h_{i-\frac{1}{2}}}{2},$$

we find

$$\frac{h_{i+\frac{1}{2}} - \delta x_i}{0.5(\tilde{h}_{i+\frac{1}{2}} + \tilde{h}_{i-\frac{1}{2}})} < 2 \quad \text{or} \quad \Delta x_i \leq 2 \cdot \delta x_i.$$

Now we see that (5.25) will be satisfied if

$$2\delta x_i \leq \frac{\tilde{h}_{i+\frac{1}{2}}}{2} = \frac{h_{i+\frac{1}{2}} + \delta x_{i+1} - \delta x_i}{2}. \tag{5.31}$$

Analysis of (5.31) shows that a sufficient condition to ensure this inequality is

$$\delta x_i < \frac{h_{i+\frac{1}{2}}}{6}, \quad |\delta x_{i+1}| < \frac{h_{i+\frac{1}{2}}}{6} \tag{5.32}$$

or, in terms of the new coordinates,

$$x_i - \frac{x_i - x_{i-1}}{6} < \tilde{x}_i < x_i + \frac{x_{i+1} - x_i}{6}. \tag{5.33}$$

To summarize, our mc method requires a more restrictive condition on the displacements than *SFB/DC*; it is not monotone, because the coefficients of the various density terms do not sum to 1. However the mc method is positive definite because all coefficients are positive, has a higher order of accuracy than *SFB/DC*, and is conservative because it is written in flux form.

Although ρ^{mc} does not preserve monotonicity of ρ^{da} , the individual values are positive and bounded from above. That is, using the fact that all ρ^{da} and $\tilde{h}_{i+\frac{1}{2}}$ are positive, and that the total mass is conserved, we can write for any particular cell $j + \frac{1}{2}$

$$\rho_{j+\frac{1}{2}}^{\text{mc}} \cdot \tilde{h}_{j+\frac{1}{2}} \leq \sum_{\text{cells}} \rho_{i+\frac{1}{2}}^{\text{mc}} \cdot \tilde{h}_{i+\frac{1}{2}} = M \quad \text{and so} \quad \rho_{j+\frac{1}{2}}^{\text{mc}} \leq \frac{M}{\tilde{h}_{i+\frac{1}{2}}}.$$

Clearly more accurate estimates would be useful: however, the estimates above guarantee that the mc method is stable in the sense that it cannot produce unbounded densities.

5.2. 2D error analysis and compensation

Here we extend the analysis of the previous subsection to two dimensions and a logically rectangular grid. Our goal is to derive a 2D version of the mc remapping; i.e., a two-pass process in which the first step is the da algorithm, and the second step is a compensation of the second-order error, and that is both conservative and positivity preserving.

To analyze the error in the SFB/DC method in 2D, we write the difference between the exact mass and the donor-cell mass

$$m_{i+\frac{1}{2},j+\frac{1}{2}}^{\text{ex}} - m_{i+\frac{1}{2},j+\frac{1}{2}}^{\text{da}} = (e_{i+1,j+\frac{1}{2}}^{\text{ex}} - e_{i,j+\frac{1}{2}}^{\text{ex}}) + (e_{i+\frac{1}{2},j+\frac{1}{2}}^{\text{ex}} - e_{i+\frac{1}{2},j}^{\text{ex}}),$$

where

$$e_{i,j+\frac{1}{2}}^{\text{ex}} = \mathcal{F}_{i,j+\frac{1}{2}}^{\text{ex}} - \mathcal{F}_{i,j+\frac{1}{2}}^{\text{da}}, \quad e_{i+\frac{1}{2},j}^{\text{ex}} = \mathcal{F}_{i+\frac{1}{2},j}^{\text{ex}} - \mathcal{F}_{i+\frac{1}{2},j}^{\text{da}}.$$

The center of volume of the cell $C_{i+\frac{1}{2},j+\frac{1}{2}}$ is the point

$$P_{i+\frac{1}{2},j+\frac{1}{2}} = (x_{i+\frac{1}{2},j+\frac{1}{2}}, y_{i+\frac{1}{2},j+\frac{1}{2}}),$$

where

$$x_{i+\frac{1}{2},j+\frac{1}{2}} = \frac{\int_{C_{i+\frac{1}{2},j+\frac{1}{2}}} x dV}{V(C_{i+\frac{1}{2},j+\frac{1}{2}})}, \quad y_{i+\frac{1}{2},j+\frac{1}{2}} = \frac{\int_{C_{i+\frac{1}{2},j+\frac{1}{2}}} y dV}{V(C_{i+\frac{1}{2},j+\frac{1}{2}})}. \tag{5.34}$$

The coordinates of these points can be computed exactly, see Section 4.1.

Because $\rho_{i+\frac{1}{2},j+\frac{1}{2}} = \rho(x_{i+\frac{1}{2},j+\frac{1}{2}}, y_{i+\frac{1}{2},j+\frac{1}{2}}) + O(h^2)$, we can write

$$\rho(x, y) = \rho_{i+\frac{1}{2},j+\frac{1}{2}} + \left. \frac{\partial \rho}{\partial x} \right|_{P_{i+\frac{1}{2},j+\frac{1}{2}}} \cdot (x - x_{i+\frac{1}{2},j+\frac{1}{2}}) + \left. \frac{\partial \rho}{\partial y} \right|_{P_{i+\frac{1}{2},j+\frac{1}{2}}} \cdot (y - y_{i+\frac{1}{2},j+\frac{1}{2}}) + O(h^2). \tag{5.35}$$

Let us assume that $V(\delta F_{i,j+\frac{1}{2}}) > 0$, i.e., that most of the swept region belongs originally to cell $C_{i+\frac{1}{2},j+\frac{1}{2}}$.

Inserting the density distribution (5.35) into the exact flux $\int_{\delta F_{i,j+\frac{1}{2}}} \rho dV$, and then subtracting the donor-cell flux defined in (4.17) and (4.18), we find the error

$$e_{i,j+\frac{1}{2}}^{\text{ex}} = \left. \frac{\partial \rho}{\partial x} \right|_{P_{i+\frac{1}{2},j+\frac{1}{2}}} \cdot \int_{\delta F_{i,j+\frac{1}{2}}} (x - x_{i+\frac{1}{2},j+\frac{1}{2}}) dV + \left. \frac{\partial \rho}{\partial y} \right|_{P_{i+\frac{1}{2},j+\frac{1}{2}}} \cdot \int_{\delta F_{i,j+\frac{1}{2}}} (y - y_{i+\frac{1}{2},j+\frac{1}{2}}) dV + O(h^4). \tag{5.36}$$

Because of the estimate

$$\left. \frac{\partial \rho}{\partial x} \right|_{P_{i+\frac{1}{2},j+\frac{1}{2}}} = \left. \frac{\partial \rho}{\partial x} \right|_{P_{i,j+\frac{1}{2}}} + O(h),$$

we can rewrite (5.36) using the partial derivatives of ρ evaluated at the middle of the face $-P_{i,j+\frac{1}{2}}$:

$$e_{i,j+\frac{1}{2}}^{\text{ex}} = \left. \frac{\partial \rho}{\partial x} \right|_{P_{i,j+\frac{1}{2}}} \cdot \int_{\delta F_{i,j+\frac{1}{2}}} (x - x_{i+\frac{1}{2},j+\frac{1}{2}}) dV + \left. \frac{\partial \rho}{\partial y} \right|_{P_{i,j+\frac{1}{2}}} \cdot \int_{\delta F_{i,j+\frac{1}{2}}} (y - y_{i+\frac{1}{2},j+\frac{1}{2}}) dV + O(h^4). \tag{5.37}$$

Eq. (5.37) will be more convenient in future analysis. Similar formulas hold for each of the other cell faces, with appropriate changes of index (which also depends on the sign of the swept volumes). From (5.37), we recognize that $e_{i,j+\frac{1}{2}}^{\text{ex}} = O(h^3)$ and therefore overall accuracy of donor-cell method for masses is $O(h^3)$. Furthermore, since

$$\rho_{i+\frac{1}{2},j+\frac{1}{2}}^{\text{da}} = \frac{m_{i+\frac{1}{2},j+\frac{1}{2}}^{\text{da}}}{V(C_{i+\frac{1}{2},j+\frac{1}{2}})},$$

and $V(C_{i+\frac{1}{2},j+\frac{1}{2}}) = O(h^2)$, the da method for density has first-order accuracy.

In analogy to the 1D case, we estimate the error by approximating the density derivatives $\partial\rho/\partial x$ and $\partial\rho/\partial y$. It is most natural to define the discrete analogs of derivatives at the nodes. For any plane region Ω , we have by Green’s theorem

$$\int_{\Omega} \frac{\partial\rho}{\partial x} dx dy = \oint_{\partial\Omega} \rho dy.$$

We define the centers of the sides by

$$P_{i+\frac{1}{2},j}, = [0.5(x_{i,j} + x_{i+1,j}), 0.5(y_{i,j} + y_{i+1,j})], \quad P_{i,j+\frac{1}{2}} = [0.5(x_{i,j} + x_{i,j+1}), 0.5(y_{i,j} + y_{i,j+1})].$$

Next, we construct a contour that is an octagon around each node by connecting the centers of volume of the surrounding cells, and the centers of the sides. The nodal volume (see Fig. 6) is defined

$$V_{i,j} \equiv V \left(\left\{ P_{i+\frac{1}{2},j+\frac{1}{2}}, P_{i,j+\frac{1}{2}}, P_{i-\frac{1}{2},j+\frac{1}{2}}, P_{i-\frac{1}{2},j}, P_{i-\frac{1}{2},j-\frac{1}{2}}, P_{i,j-\frac{1}{2}}, P_{i+\frac{1}{2},j-\frac{1}{2}}, P_{i+\frac{1}{2},j} \right\} \right).$$

Using Green’s theorem, we obtain following approximation for $\partial\rho/\partial x$ (see [30] for details):

$$\begin{aligned} \left(\frac{\partial\rho}{\partial x} \right)_{i,j} &= \frac{1}{V_{i,j}} \cdot \left(\rho_{i+\frac{1}{2},j+\frac{1}{2}}(y_{i,j+\frac{1}{2}} - y_{i+\frac{1}{2},j}) + \rho_{i-\frac{1}{2},j+\frac{1}{2}}(y_{i-\frac{1}{2},j} - y_{i,j+\frac{1}{2}}) \right. \\ &\quad \left. + \rho_{i-\frac{1}{2},j-\frac{1}{2}}(y_{i,j-\frac{1}{2}} - y_{i-\frac{1}{2},j}) + \rho_{i+\frac{1}{2},j-\frac{1}{2}}(y_{i+\frac{1}{2},j} - y_{i,j-\frac{1}{2}}) \right). \end{aligned} \tag{5.38}$$

A similar equation can be derived for the approximation of $\partial\rho/\partial y$ at the node. We also define the average value of density at the node as

$$\rho_{i,j} = \frac{\rho_{i+\frac{1}{2},j+\frac{1}{2}} + \rho_{i-\frac{1}{2},j+\frac{1}{2}} + \rho_{i-\frac{1}{2},j-\frac{1}{2}} + \rho_{i+\frac{1}{2},j-\frac{1}{2}}}{4}.$$

Continuing the analogy with the 1D presentation, we define the volume of the pseudo swept region of the face $(i, j + \frac{1}{2})$ as

$$\begin{aligned} V_{i,j+\frac{1}{2}} &= \frac{1}{2} \left[\left(\frac{\delta\rho}{\delta x} \right)_{i,j} / \rho_{i,j} + \left(\frac{\delta\rho}{\delta x} \right)_{i+1,j} / \rho_{i+1,j} \right] \cdot \left(\int_{\delta F_{i,j+\frac{1}{2}}} (x - x_{i+\frac{1}{2},j+\frac{1}{2}}) dV \right) \\ &\quad + \frac{1}{2} \left[\left(\frac{\delta\rho}{\delta y} \right)_{i,j} / \rho_{i,j} + \left(\frac{\delta\rho}{\delta y} \right)_{i+1,j} / \rho_{i+1,j} \right] \cdot \left(\int_{\delta F_{i,j+\frac{1}{2}}} (y - y_{i+\frac{1}{2},j+\frac{1}{2}}) dV \right). \end{aligned} \tag{5.39}$$

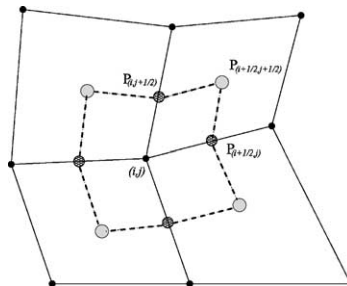


Fig. 6. Control volume $V_{i,j}$ and its pieces, used to discretize derivatives $\partial\rho/\partial x$, and $\partial\rho/\partial y$ and average ρ at the node (i, j) . Boundary of volume $V_{i,j}$ is dashed line.

Similar formulas can be derived for the other cell faces. Using these pseudo volumes, the second pass in the mc method is written as

$$m_{i+\frac{1}{2},j+\frac{1}{2}}^{mc} = m_{i+\frac{1}{2},j+\frac{1}{2}}^{da} + \mathcal{F}_{i+1,j+\frac{1}{2}}^{mc} - \mathcal{F}_{i,j+\frac{1}{2}}^{mc} + \mathcal{F}_{i+\frac{1}{2},j+1}^{mc} - \mathcal{F}_{i+\frac{1}{2},j}^{mc},$$

where the “mc-fluxes” are

$$\mathcal{F}_{i,j+\frac{1}{2}}^{mc} = \rho_{i,j+\frac{1}{2}}^{da} \cdot V_{i,j+\frac{1}{2}}, \quad \mathcal{F}_{i+\frac{1}{2},j}^{mc} = \rho_{i+\frac{1}{2},j}^{da} \cdot V_{i+\frac{1}{2},j}. \tag{5.40}$$

The density on a face depends on the sign of the volume of its associated pseudo swept region similar to formulas (5.22) in 1D

$$\rho_{i,j+\frac{1}{2}}^{da} = \begin{cases} \rho_{i+\frac{1}{2},j+\frac{1}{2}}^{da}, & V_{i,j+\frac{1}{2}} \geq 0, \\ \rho_{i-\frac{1}{2},j+\frac{1}{2}}^{da}, & V_{i,j+\frac{1}{2}} < 0, \end{cases} \quad \rho_{i+\frac{1}{2},j}^{da} = \begin{cases} \rho_{i+\frac{1}{2},j+\frac{1}{2}}^{da}, & V_{i+\frac{1}{2},j} \geq 0, \\ \rho_{i+\frac{1}{2},j-\frac{1}{2}}^{da}, & V_{i+\frac{1}{2},j} < 0. \end{cases} \tag{5.41}$$

One can easily prove that $\mathcal{F}^{mc} = e^{ex} + O(h^4)$, and so the 2D mc method is fourth-order accurate for masses and second-order accurate with respect to ρ .

As in 1D, there are other choices for defining the volumes of the pseudo swept regions. One possibility is described in [24], where the method of Barth and Jespersen [3] is used to approximate cell-centered derivatives. We denote the results of the corresponding method by mb. Formally, the mb method has the same order of accuracy as the mc method. In numerical examples, we will show that the mb method improves the preservation of monotonicity of the remapping and relaxes requirements on the displacement field. However, as is the case for the mm method in 1D the mb method produces less sharp profiles compared to the mc method.

The condition that the second pass of our 2D mc method preserves positivity is that the sum of all negatively signed volumes of the pseudo swept regions associated with $\tilde{C}_{i+\frac{1}{2},j+\frac{1}{2}}$ do not exceed $V(\tilde{C}_{i+\frac{1}{2},j+\frac{1}{2}})$.

These volumes depend on both the original displacement field and on the density field itself. As in the 1D case, it is possible to show that the preservation of positivity during the second pass can be enforced with a condition like

$$|V_{i,j+\frac{1}{2}}| \leq CV(\delta F_{i,j+\frac{1}{2}}),$$

where C is a constant independent of h (see [24]). The value of this constant will depend on the geometrical properties of the old grid, as well as the rezone procedure that leads to the new grid. Unfortunately, it is more difficult to explicitly determine this constant in 2D, and a more practical solution is to enforce positivity during the simulation.

All of the qualitative conclusions that we have made about the mc method in 1D hold in 2D as well: it is second-order accurate: it is not monotone but is positivity preserving and conservative, and so produces densities that are bounded from above.

6. Numerical results

Our remapping algorithm is intended to be coupled with a rezoner, and used in the context of ALE simulations. However it is instructive to test it in a simpler environment, where there are no partial differential equations, nor any Lagrangian algorithm. We will test the remapper in the context of interpolation. That is, we will choose an underlying function, prescribe a grid motion, and compare the

exact integrals of this function on the new grids to the numerical simulations. We consider examples of logically rectangular grids and unstructured grids in 2D. Additional examples in 1D and 2D can be found in [24].

6.1. Cyclic remapping

Here, we assume that we have a sequence of grids $\{x_I^n, I = 1, \dots, I_{\max}; n = 0, \dots, n_{\max}\}$, where the subscript I represents multiple indices, which identify a point, on the grid (structured or unstructured), and the superscript identifies a particular grid. It is convenient to think of the index n as representing a fictitious time t^n , which is a parameter to define the grid motion. We begin with a test function $\rho(x, y)$ and compute its means on grid x_I^0 , then remap the function means from grid x_I^0 to grid x_I^1 , and then remap resulting means from grid x_I^1 to grid x_I^2 , etc. This allows us to look at the cumulative effects of many remappings.

Let us note that in our real calculations instead of computing integral averages over cells we just compute its value at the center of mass, which is equal to the integral average with second-order accuracy.

6.2. 2D structured grids

Here, we test the da, mp and mb methods on 2D logically rectangular, structured grids (n.b. the mb method is described in [24]). We assume a sequence of grids

$$x_{i,j}^n, \quad i = 1, \dots, i_{\max}, \quad j = 1, \dots, j_{\max}; \quad n = 0, \dots, n_{\max};$$

where the subscripts identify the cell and the superscript identifies a particular grid in the sequence. In all our tests we take $i_{\max} = j_{\max}$, and therefore in all figure captions we state only i_{\max} and n_{\max} .

6.2.1. Tensor product grids

For our first series of tests, we generate a sequence of smooth grids in the unit square $[0, 1] \times [0, 1]$, using the functions

$$\begin{aligned} x(\xi, \eta, t) &= (1 - \alpha(t))\xi + \alpha(t)\xi^3, & y(\xi, \eta, t) &= (1 - \alpha(t))\eta + \alpha(t)\eta^2, \\ \alpha(t) &= \frac{\sin(4\pi t)}{2}, & 0 \leq \xi \leq 1; & \quad 0 \leq \eta \leq 1; & \quad 0 \leq t \leq 1. \end{aligned} \quad (6.1)$$

This produces a sequence of tensor product grids grid $\{x_{i,j}^n\}$, given by

$$x_{i,j}^n = x(\xi_i, \eta_j, t^n), \quad y_{i,j}^n = y(\xi_i, \eta_j, t^n), \quad (6.2)$$

where $t^n = n/n_{\max}$, $n = 0, \dots, n_{\max}$; and

$$\xi_i = (i - 1)/(i_{\max} - 1), \quad i = 1, \dots, i_{\max}, \quad \eta_j = (j - 1)/(j_{\max} - 1), \quad j = 1, \dots, j_{\max}.$$

For $t = t^0 = 0$, and $t = t^n = 1$, $\alpha(t)$ is zero so that the initial and final grids are identical and uniform. In Fig. 7. we show two intermediate grids. The first panel, Fig. 7(a), corresponds to a pseudo time $t = 0.375$, when the grid is stretched toward the top and right. The second panel, Fig. 7(b), corresponds to a pseudo time $t = 0.625$, when the grid is stretched toward the bottom and left.

We compare three methods for remapping on the sequence of the grids given by (6.1), the da method, the mc method, and the mb method. Our first density represents a smooth function and is given by: $\rho(x, y) = 1 + \sin(2\pi x) \sin(2\pi y)$. We term these the ‘‘sine’’ tests. We use three different levels of refinement to investigate convergence: $i_{\max} = j_{\max} = 65, 129, 257$ with a corresponding number of pseudo time steps,

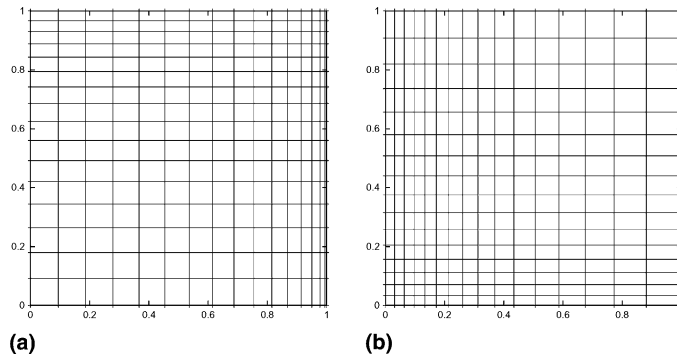


Fig. 7. Two intermediate grids for tensor product grid movement, $i_{\max} = 17, j_{\max} = 17$: (a) $t = 0.375$; (b) $t = 0.625$.

$n_{\max} = 320, 640, 1280$, respectively. In Fig. 8 we show isolines for density at the final time $n_{\max} = 320, i_{\max} = j_{\max} = 65$.

The da method produces an overly smoothed solution and the isolines are very distorted. The mc and mb methods produce better and qualitatively very similar results.

To investigate convergence and compare the methods quantitatively, we use the two norms:

$$\|\rho^* - \rho\|_{\max} = \max_{i,j} |\rho^h_{i+\frac{1}{2},j+\frac{1}{2}} - \rho(x_{i+\frac{1}{2},j+\frac{1}{2}}, y_{i+\frac{1}{2},j+\frac{1}{2}})|, \tag{6.3}$$

$$\|\rho^* - \rho\|_{L_1} = \sum_{i,j} \left\{ |\rho^h_{i+\frac{1}{2},j+\frac{1}{2}} - \rho(x_{i+\frac{1}{2},j+\frac{1}{2}}, y_{i+\frac{1}{2},j+\frac{1}{2}})| \cdot V(C_{i+\frac{1}{2},j+\frac{1}{2}}) \right\}.$$

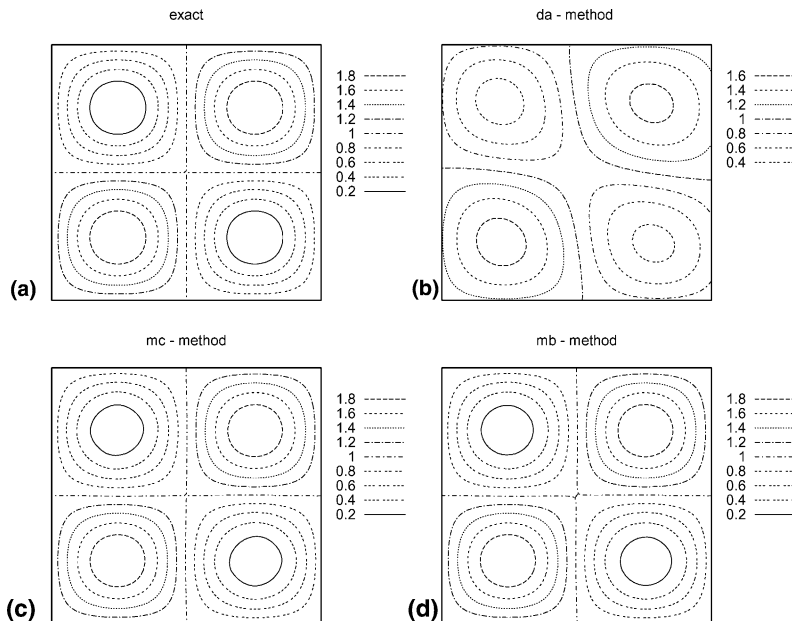


Fig. 8. Results for $\rho(x, y) = 1 + \sin(2\pi x) \sin(2\pi y)$ and smooth displacements field given by (6.1), isolines.

Table 1
The errors in max and L_1 norm for the sine tests and smooth displacement field

i_{\max}/n_{\max}	Norm	da	mc	mb
65/320	L_1	0.133	$9.77\text{E}-3$	$1.04\text{E}-2$
	max	0.364	$6.91\text{E}-2$	$8.43\text{E}-2$
129/640	L_1	$7.73\text{E}-2$	$2.54\text{E}-3$	$2.63\text{E}-3$
	max	0.214	$2.82\text{E}-2$	$3.39\text{E}-2$
257/1280	L_1	$4.19\text{E}-2$	$6.40\text{E}-4$	$6.53\text{E}-4$
	max	0.117	$1.13\text{E}-2$	$1.32\text{E}-2$

In Table 1, we summarize the convergence results for the sine function and the sequence of tensor product grids. The table shows that the da method has first-order convergence in both norms, whereas both the mc and mb methods show second-order convergence in L_1 norm, and slightly less than second-order in max norm.

The second density will be termed the “peak” function and is defined

$$\rho(x, y) = \begin{cases} 0, & r > 0.25, \\ \max(0.001, 4(r - 0.25)), & r \leq 0.25, \end{cases} \quad r = \sqrt{(x - 0.5)^2 + (y - 0.5)^2}. \quad (6.4)$$

This function is shown in Fig. 9, where we also present surface plots for the remapped function. The corresponding isolines are shown in Fig. 10. The da method produces poor results. The mb method overly smooths the peak compared with the mc method.

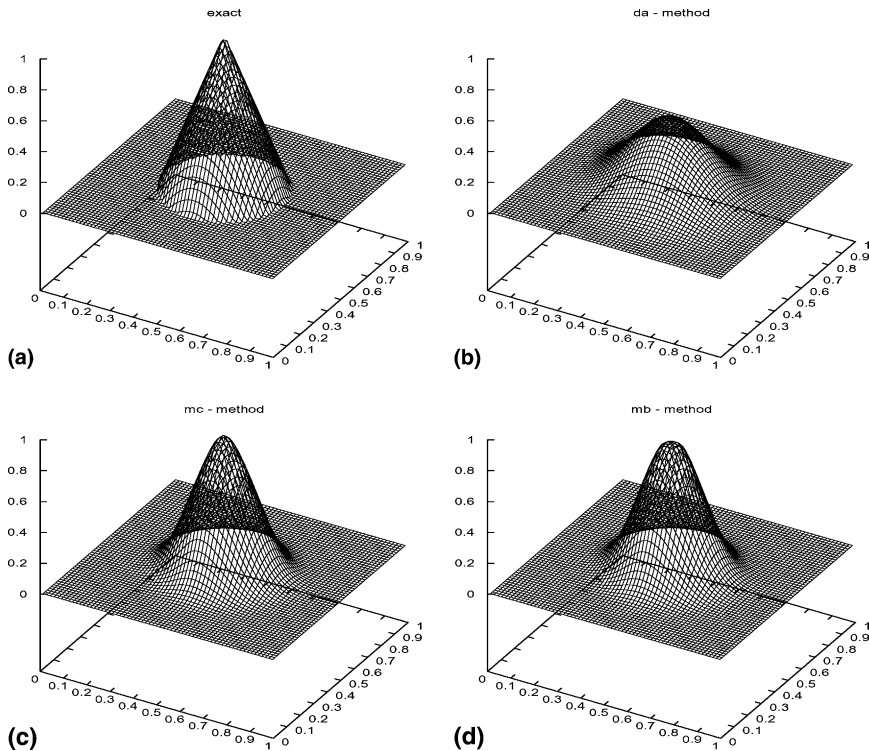


Fig. 9. Numerical results for the peak function, $n_{\max} = 320$, $i_{\max} = j_{\max} = 65$, surface plots.

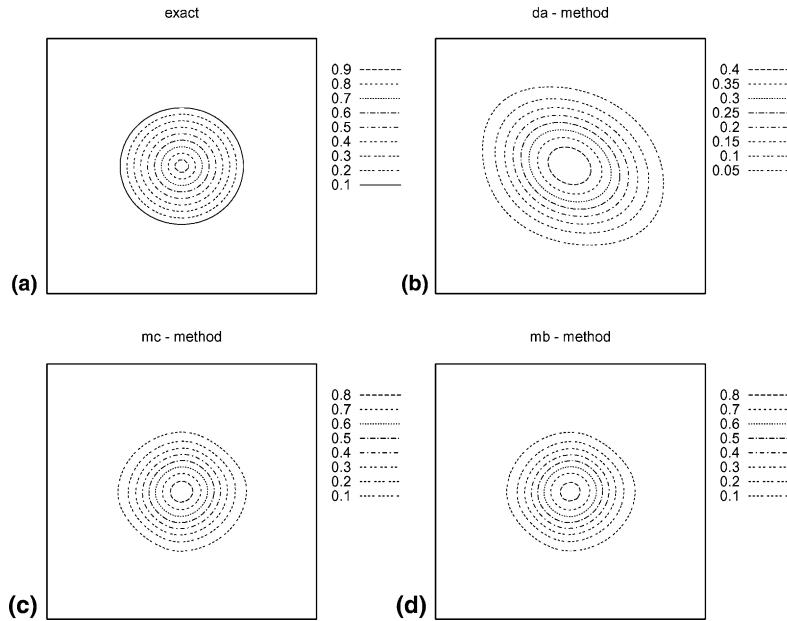


Fig. 10. Results for the peak test function and sequence of tensor product grids, isolines.

In Table 2 we summarize the convergence results for the peak density. Here we use only the L_1 norm. The table shows that the da method shows somewhat less than first-order convergence, while both the mc method and mb methods show slightly more than first-order. Perhaps of greater significance, both the mc and mb methods have almost an order of magnitude smaller error.

The third density function we use represents an oblique shock and will be termed the “shock” test. It is defined as

$$\rho(x,y) = \begin{cases} 1, & y > (x - 0.4)/0.3, \\ 0, & y \leq (x - 0.4)/0.3. \end{cases} \tag{6.5}$$

The isolines for the shock density are shown in Fig. 11, where we also present the results of the different remappings for this test. The qualitative conclusion from these pictures is the same as for previous tests. However one can see the relatively greater loss of monotonicity in the mc method compared to the mb method.

In Table 3 we summarize the convergence results for the shock density test. Here, all methods are slightly less than first-order accurate, with the m methods exhibiting about a twice smaller error than the da method.

Table 2
The errors in L_1 norm for the peak density function and sequence of tensor product grids

i_{\max}/n_{\max}	Norm	da	mc	mb
65/320	L_1	4.02E-02	9.01E-3	9.64E-3
129/640	L_1	2.48E-2	3.76E-3	3.99E-3
257/1280	L_1	1.42E-2	1.52E-3	1.61E-3

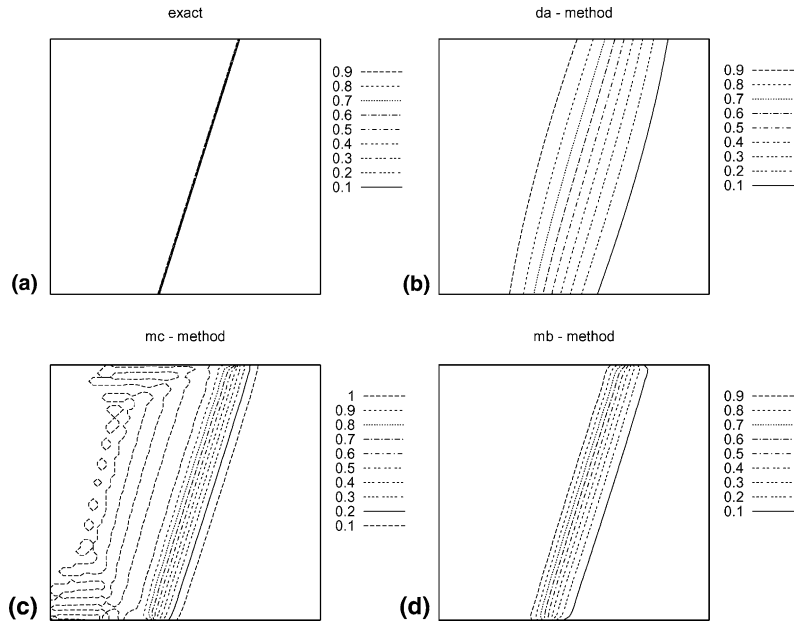


Fig. 11. Isolines of the shock test function and sequence of tensor product grids.

Table 3
The errors in L_1 norm for the shock test and tensor product grids

i_{\max}/n_{\max}	Norm	da	mc	mb
65/320	L_1	0.109	$4.56E-2$	$4.73E-2$
129/640	L_1	$7.78E-2$	$2.88E-2$	$2.97E-2$
257/1280	L_1	$5.51E-2$	$1.82E-2$	$1.86E-2$

6.2.2. Random grids

Here, we use a sequence of random grids in which each grid is obtained by an independent random perturbation of a uniform grid

$$x_{i,j}^n = \xi_i + \gamma r_i^n h, \quad y_{i,j}^n = \eta_j + \gamma r_j^n h, \tag{6.6}$$

where $-0.5 \leq r_i^n, r_j^n \leq 0.5$ are random numbers. In Fig. 12 we show two realizations of these random grids for $i_{\max} = j_{\max} = 17$, for $\gamma = 0.5$ and 0.7 . In this case, all grids are random and it is unlikely that we will ever return to the original grid. Strictly speaking then, we cannot use these tests to measure convergence rate. For the sine and peak test functions, the results are similar to those for tensor product grids for this test function, and so we do not present them here (complete numerical results are presented in [24]). We note that these results are more accurate than for the case of sequence of tensor product grids. Possibly the random sequence of grids does not allow a systematic buildup of remapping error.

For the shock test function and sequence of random grids with $\gamma = 0.5$ the results are also similar to one for tensor product grids and are not presented here, see [24]. If we increase the parameter γ , which regulates the degree of randomness, to 0.7 , thus allowing larger displacements, then for the shock test function the mc method produces negative densities. However the da and mb methods continue to produce only positive densities. The corresponding graphs for these methods are presented in Fig. 13. This example demonstrates that, in general, the mb method allows larger displacements than the mc method.

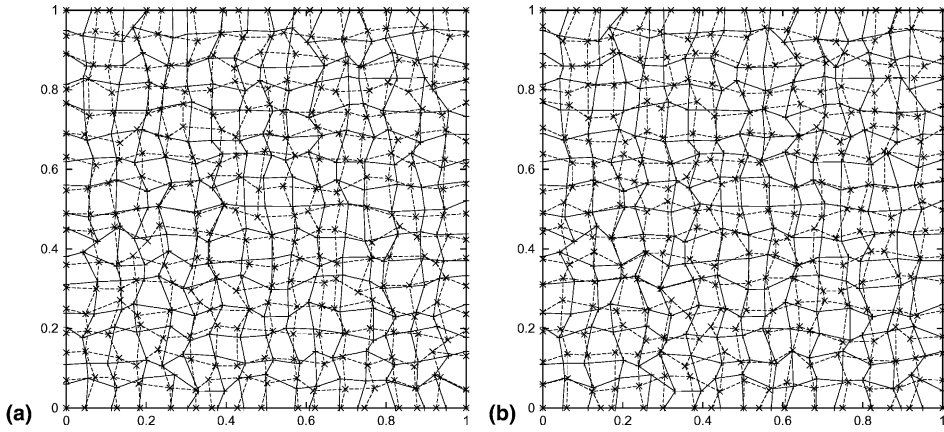


Fig. 12. Two consecutive random grids: (a) $\gamma = 0.5$; (b) $\gamma = 0.7$

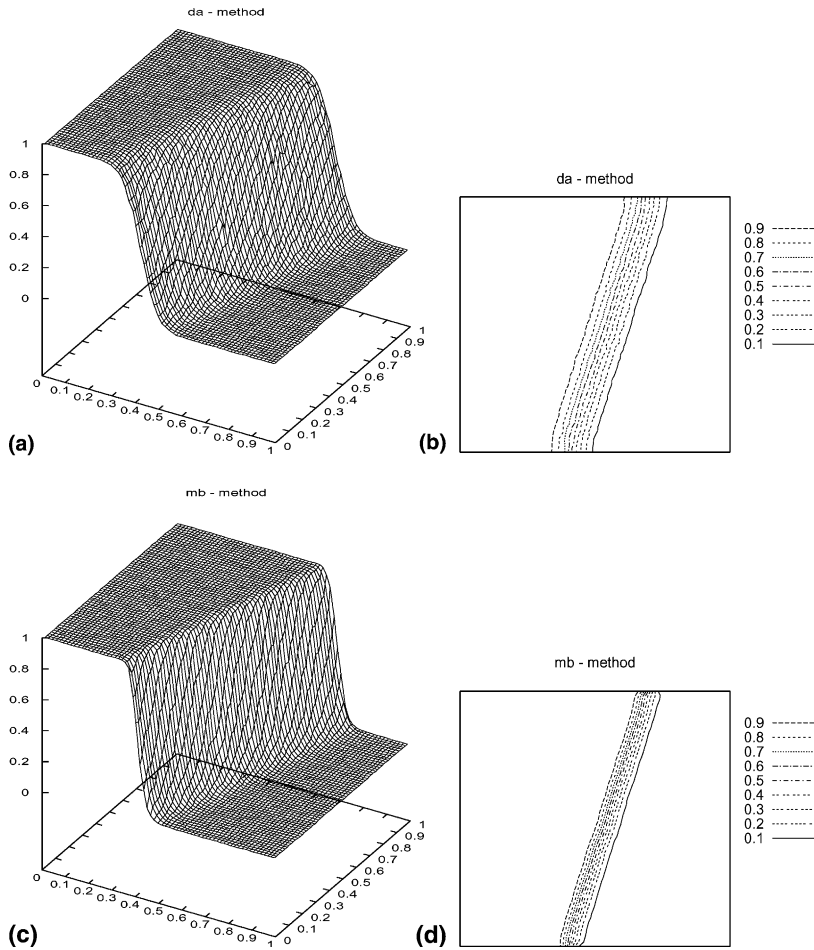


Fig. 13. Results for the shock function, $n_{\max} = 100$, $i_{\max} = j_{\max} = 65$, and a sequence of random grids, $\gamma = 0.7$.

Table 4
The errors in L_1 norm for the shock test and random grid movement, $\gamma = 0.7$

i_{\max}/n_{\max}	Norm	da	mb
65/100	L_1	4.90E-2	2.71E-2
129/100	L_1	2.45E-2	1.36E-2

The L_1 errors for this case is presented in Table 4. Note that we present here results only for $i_{\max} = j_{\max} = 65$ and $= 129$. At $i_{\max} = j_{\max} = 257$, both the da and mb methods start to produce small, negative densities.

6.2.3. Consecutive smoothing of an initially random grid

In last series of tests for structured grids we consider a sequence of grids that more closely simulates a realistic situation in an ALE simulation. Here each grid in the sequence is obtained from the previous one by smoothing

$$x_{i,j}^{n+1} = \frac{(x_{i-1,j}^n + 2x_{i,j}^n + x_{i+1,j}^n) + (x_{i,j-1}^n + 2x_{i,j}^n + x_{i,j+1}^n)}{8}$$

and similar formula for y . In our experiment, the initial grid is obtained from a uniform grid by random perturbation

$$x_{i,j}^0 = \zeta_i + r_i h, \quad y_{i,j}^0 = \eta_j + r_j h. \tag{6.7}$$

Here, $-0.25 \leq r_i, r_j \leq 0.25$ are random numbers, and $h = 1/(i_{\max} - 1)$. For nodes on the boundary of the unit square, only one coordinate is perturbed. The initial grid, the grid after one smoothing and after 20 smoothing are shown in Fig. 14.

For this sequence of grids, we present remapping results only for the peak function. The results in Table 5 show a convergence rate slightly higher than first order for the da method, and slightly less than second order for the mc method. Graphically, the remapped density is not distinguishable from the exact density, and so is not shown.

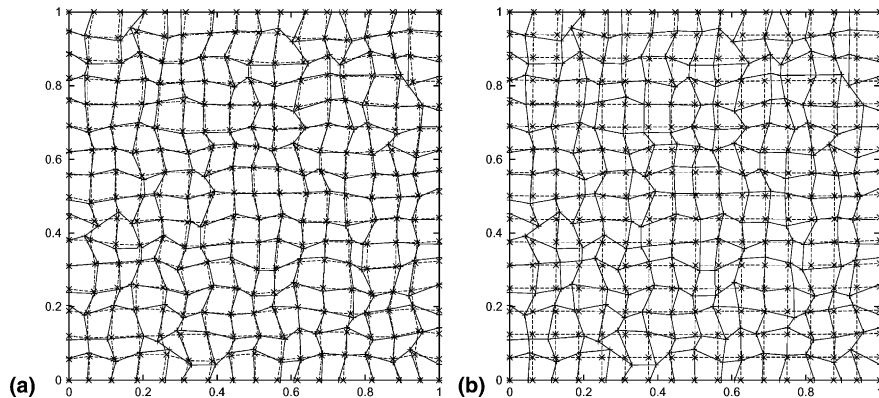


Fig. 14. Smoothing $i_{\max} = 17, j_{\max} = 17$: (a) initial grid, and grid after one step of smoothing; (b) initial grid and “final grid” after 20 smoothing steps.

Table 5
The errors in L_1 norm for peak test function and a sequence of grids obtained by consecutive smoothing

i_{\max}/η_{\max}	Norm	da	mc	mb
65/20	L_1	6.05E-4	1.69E-4	2.12E-4
129/20	L_1	2.80E-4	4.92E-5	4.92E-5
257/20	L_1	1.37E-4	1.34E-5	1.84E-5

6.3. Unstructured grids

In this section we will describe the results of remapping the peak density on a sequence of unstructured grids obtained by consecutive smoothing. The initial grid is constructed in a series of steps. First, for a given integer m we create points inside the unit square with the coordinates

$$x_{i,j} = \left(\xi_i + (-1)^{i+j} \cdot \frac{h}{4} \right)^2, \quad y_{i,j} = \left(\eta_j + (-1)^{i+j+1} \cdot \frac{h}{10} \right)^2,$$

$$\xi_i = (i - 0.5)h, \quad \eta_j = (j - 0.5)h, \quad i, j = 1, \dots, m; \quad h = 1/m.$$

Next, we use this set of points to construct Voronoi cells, which surround the point. At each point P , the associated Voronoi cell consists of that part of the plane in which all points are closer to P than to any other point of the set. See, for example, [12,27] for additional details. The important topological property of this tessellation is that exactly three edges meet at each vertex. In principle, degenerate cases in which edges of zero length can exist. At this stage, we have a grid consisting of Voronoi cells, whose vertices define Voronoi polygons. Finally, we square all the coordinates of the vertices. The resulting grid is shown in Fig. 15(a). Our smoothing procedure for these unstructured grids is:

$$x_k^{n+1} = x_k^n + \alpha \cdot \frac{x_{k_1}^n + x_{k_2}^n + x_{k_3}^n - 3x_k^n}{3}, \quad k \text{ internal vertex},$$

$$x_k^{n+1} = x_k^n + \alpha \cdot \frac{x_{k_1}^n + x_{k_2}^n - 2x_k^n}{2}, \quad k \text{ boundary vertex},$$

where the stencils for smoothing the internal and boundary are nodes of the sides sharing vertex k . The nodes in the corners of the computational domain are fixed. The final grid after 2500 smoothing steps is shown in Fig. 15(b).

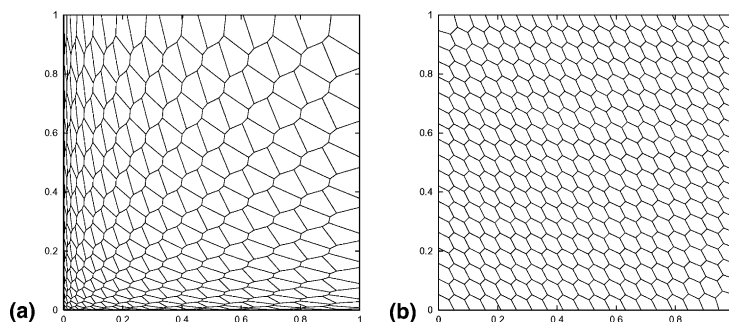


Fig. 15. Initial and final unstructured grid, for $m = 19$: (a) initial grid; (b) “final grid” after 2500 smoothing steps.

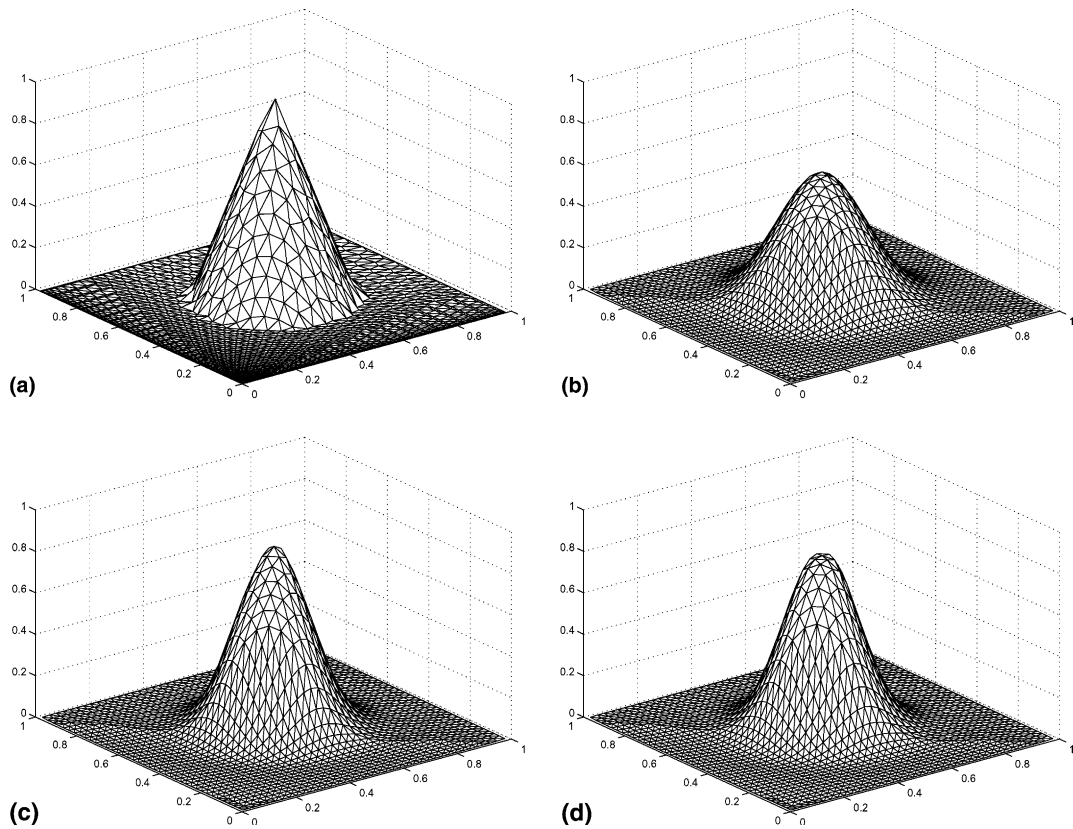


Fig. 16. Remapping of peak test function on unstructured grids $m = 39$ and 5000 smoothing steps: (a) function on initial grid; (b) remap by the da method; (c) remap by the mc method; (d) remap by the mb method.

Table 6

The errors in L_1 norm for peak test function on an unstructured grids

m/η_{\max}	Norm	da	mc	mb
19/2500	L_1	4.49E-2	2.21E-2	2.43E-2
39/5000	L_1	2.31E-2	8.93E-3	9.45E-3

The results of remapping the peak density are presented in Fig. 16. These plots are produced by MATLAB [20]. The data are the values of density at the centers of volume of the Voronoi cells. MATLAB performs its own triangulation (using the *delaunay* utility) to draw surfaces (using *trimesh*). Thus, the vertices of the grid shown in Fig. 16 are the centers of volume of our original mesh.

The results of a convergence study are presented in Table 6. The behavior of each method on the unstructured grid is similar to that on the structured grids. The da method shows first-order convergence while the mc and mb methods show second-order convergence. The mc method produces the sharper peak.

7. Summary

In this paper we have constructed a second-order accurate, sign preserving, conservative interpolation (remapping) algorithm suitable for use in continuous rezone ALE schemes, and applicable to both

structured and unstructured grids. The final scheme consists of two passes through the set of faces of the grid. The first pass applies first-order accurate estimates of the remap fluxes to construct a first-order remapping. The second pass estimates and compensates the lowest-order errors to improve the solution to second-order accuracy. These estimates are based on the sign of the swept regions, and ensure sign preservation in the overall solution.

Within the estimates of the second-order error, we have the option of how to approximate local density derivatives. We consider two choices, one based on central differencing and the other based on linear reconstruction with limiting. In a series of problems, we show that both choices exhibit second-order convergence for smooth densities. For nonsmooth and discontinuous densities, we show that both choices have very similar performance, with the central differencing being slightly more accurate and the Barth's differences being slightly less oscillatory. Both second-order accurate schemes are considerably more accurate than the associated single pass scheme.

Acknowledgements

This work was performed under the auspices of the US Department of Energy at Los Alamos National Laboratory, under contract W-7405-ENG-36. The authors acknowledge the partial support of the DOE/BES Program in the Applied Mathematical Sciences and the Laboratory Directed Research and Development program (LDRD). M. Shashkov also acknowledges the partial support of DOE's Accelerated Strategic Computing Initiative (ASCI). The authors thank B. Wendroff, P. Smolarkiewicz, R. Boss, T. Dey, G. Lapenta, J. Brackbill, P. Knupp, J. Dukowicz, J. Mosso, B. Swartz, and many others for fruitful discussions and constructive comments.

References

- [1] R.W. Anderson, R.B. Pember, N.S. Elliot, An arbitrary Lagrangian–Eulerian method with local structured adaptive mesh refinement for modeling shock hydrodynamics, AIAA 2002-0738, also LNL Report UCRL-JC-141625.
- [2] D.J. Benson, An efficient, accurate, simple ALE method for nonlinear finite element programs, *Comput. Methods Appl. Mech. Engrg.* 72 (1989) 305–350.
- [3] T.J. Barth, Numerical methods for gasdynamics systems on unstructured grids, in: D. Kroner, M. Ohlberger, C. Rohde (Eds.), *An Introduction to Recent Developments in Theory and Numerics for Conservation Laws*, Proceedings of the International School on Theory and Numerics for Conservation Laws, Freiburg/Littenweiler, October 20–24, 1997, Lecture Notes in Computational Science and engineering, Springer, Berlin, 1997, pp. 195–285.
- [4] D.J. Benson, Computational methods in Lagrangian and Eulerian hydrocodes, *Comput. Methods Appl. Mech. Engrg.* 99 (1992) 235–394.
- [5] D.J. Benson, Momentum advection on a staggered mesh, *J. Comput. Phys.* 100 (1992) 143–162.
- [6] P. Colella, Multidimensional upwind methods for hyperbolic conservation laws, *J. Comput. Phys.* 87 (1990) 171–200.
- [7] J. Donea, S. Giuliani, J.P. Halleux, An arbitrary Lagrangian–Eulerian finite element method for transient dynamic fluid–structure interactions, *Comput. Methods Appl. Mech. Engrg.* 33 (1982) 689–723.
- [8] J.K. Dukowicz, J.W. Kodis, Accurate conservative remapping (rezoning) for arbitrary Lagrangian–Eulerian computations, *SIAM J. Stat. Comput.* 8 (1987) 305–321.
- [9] J.K. Dukowicz, M.C. Cline, F.L. Addessio, A general topology Godunov method, *J. Comput. Phys.* 82 (1989) 29–63.
- [10] J. Dukowicz, N. Padial, REMAP3D: a conservative three-dimensional remapping code, LA-12136-MS, Report of Los Alamos National Laboratory, Los Alamos, NM, USA, 1991.
- [11] J. Dukowicz, J. Baumgardner, Incremental remapping as a transport/advection algorithm, *J. Comput. Phys.* 160 (2000) 318–335.
- [12] P.J. Frey, P.-L. George, Mesh generation, in: *Application to Finite Elements*, Chapter 2. Basic Structures and Algorithms, Hermes Science Publishing, Oxford and Paris, 2000, pp. 47–96.
- [13] J. Grandy, Conservative remapping and regions overlays by intersecting arbitrary polyhedra, *J. Comput. Phys.* 148 (1999) 433–466.

- [14] C. Hirt, A. Amsden, J. Cook, An arbitrary Lagrangian–Eulerian computing method for all flow speeds, *J. Comput. Phys.* 14 (1974) 227–253, reprinted in 135 (1997), pp. 203–216.
- [15] D.S. Kershaw, M.K. Prasad, M.J. Shaw, J.L. Milovich, 3D unstructured mesh ALE hydrodynamics with the upwind discontinuous finite element method, *Comput. Methods Appl. Mech. Engrg.* 158 (1998) 81–116.
- [16] P. Knupp, P. Knupp, M. Shashkov, Reference Jacobian optimization-based rezone strategies for arbitrary Lagrangian–Eulerian methods, *J. Comput. Phys.* 176 (2002) 93–128.
- [17] P. Kjellgren, J. Hyvarien, An arbitrary Lagrangian–Eulerian finite element method, *Comput. Mech.* 21 (1998) 81–90.
- [18] A.G. Kulikovskii, N.V. Pogorelov, A.Yu. Semenov, *Mathematical Aspects of Numerical Solution of Hyperbolic Systems*, Chapman & Hall/CRC Monographs and Surveys in Pure and Applied Mathematics, Chapter 2.7 Reconstruction Procedures and Slope Limiters, vol. 118, pp. 76–120.
- [19] H.U. Mair, Review: hydrocodes for structural response to underwater explosions, *Shock Vibr.* 6/2 (1999) 81–96.
- [20] P. Marchand, in: *Graphics and GUIs with MATLAB*, second ed., CRC Press, Boca Raton, FL, 1999, pp. 77–80.
- [21] L. Margolin, P. Smolarkiewicz, Antidiffusive velocities for multipass donor cell advection, *SIAM J. Sci. Comput.* 20 (1998) 907–929.
- [22] L.G. Margolin, C.W. Beason, Remapping on the staggered mesh, Report UCRL-99682 of Lawrence Livermore National Laboratory, 1988.
- [23] L.G. Margolin, Introduction to an arbitrary Lagrangian–Eulerian computing method for all flow speeds, *J. Comput. Phys.* 135 (1997) 198–202.
- [24] L.G. Margolin, M. Shashkov, Second-order sign-preserving remapping on general grids, Report of Los Alamos National Laboratory, LAUR-02-525 (<http://cnls.lanl.gov/~shashkov>).
- [25] S. Mosso, D. Burton, et al., A second order, two- and three-dimensional remap method, LA-UR-98-5353, Report of Los Alamos National Laboratory, Los Alamos, NM, USA, 1988.
- [26] S. Mosso, B. Swartz, An unsplit, two-dimensional advection algorithm, LA-UR-01-1476, Report of Los Alamos National Laboratory, Los Alamos, NM, USA, 2000.
- [27] A. Okabe, B. Boots, et al., *Spatial Tessellations. Concepts and Applications of Voronoi Diagrams*, second ed., Chapter 2, Definition and Basic Properties of Voronoi Diagrams. Wiley Series in Probability and Statistics, John Wiley, Chichester, England, 2000.
- [28] P.J. O'Rourke, M.S. Sahota, A variable explicit/implicit numerical method for calculating advection on unstructured meshes, *J. Comput. Phys.* 143 (1998) 312–345.
- [29] J.S. Peery, D.E. Carroll, Multi-material ALE methods in unstructured grids, *Comput. Methods Appl. Mech. Engrg.* 187 (2000) 591–619.
- [30] M. Shashkov, *Conservative Finite-difference Methods on General Grids*, CRC Press, Boca Raton, 1995.
- [31] P. Smolarkiewicz, A simple positive definite advection scheme with small implicit diffusion, *Monthly Weather Rev.* 111 (1983) 479–486.
- [32] P. Smolarkiewicz, L. Margolin, MPDATA: a finite-difference solver for geophysical flows, *J. Comput. Phys.* 140 (1998) 459–480.